

1 SEARCH FOR PRODUCTION OF A HIGGS BOSON AND A SINGLE TOP
2 QUARK IN MULTILEPTON FINAL STATES IN pp COLLISIONS AT $\sqrt{s} = 13$
3 TeV.

4 by

5 Jose Andres Monroy MontaÑez

6 A DISSERTATION

7 Presented to the Faculty of

8 The Graduate College at the University of Nebraska

In Partial Fulfilment of Requirements

10 For the Degree of Doctor of Philosophy

11 Major: Physics and Astronomy

12 Under the Supervision of Kenneth Bloom and Aaron Dominguez

13 Lincoln, Nebraska

14 July, 2018

15 SEARCH FOR PRODUCTION OF A HIGGS BOSON AND A SINGLE TOP
16 QUARK IN MULTILEPTON FINAL STATES IN pp COLLISIONS AT $\sqrt{s} = 13$
17 TeV.

18 Jose Andres Monroy Montañez, Ph.D.

19 University of Nebraska, 2018

20 Adviser: Kenneth Bloom and Aaron Dominguez

²¹ Table of Contents

²²	Table of Contents	iii
²³	List of Figures	vi
²⁴	List of Tables	viii
²⁵	1 INTRODUCTION	1
²⁶	2 Theoretical approach	2
²⁷	2.1 Introduction	2
²⁸	2.2 Standard model of particle physics	4
²⁹	2.2.1 Fermions	6
³⁰	2.2.1.1 Leptons	7
³¹	2.2.1.2 Quarks	10
³²	2.2.2 Fundamental interactions	13
³³	2.2.3 Gauge Bosons	19
³⁴	2.3 Electroweak unification and the Higgs mechanism	20
³⁵	2.3.1 Spontaneous symmetry breaking	28
³⁶	2.3.2 Higgs mechanism	32
³⁷	2.3.3 Masses of the gauge bosons	34

38	2.3.4	Masses of the fermions	35
39	2.3.5	The Higgs field	36
40	2.3.6	Higgs boson production mechanisms at LHC.	37
41	2.3.7	Higgs decay channels	40
42	2.4	Associated Production of Higgs Boson and Single Top Quark.	41
43	2.5	The CP-mixing phase	41
44	3	The CMS experiment at the LHC	42
45	3.1	Introduction	42
46	3.2	The LHC	43
47	3.3	The CMS experiment	47
48	4	Search for production of a Higgs boson and a single top quark in multilepton final states in pp collisions at $\sqrt{s} = 13$ TeV	49
50	4.1	Introduction	49
51	4.2	Data and MC Samples	51
52	4.2.1	Full 2016 dataset and MC samples	51
53	4.2.2	Triggers	54
54	4.2.2.1	Trigger efficiency scale factors	54
55	4.3	Object Identification and event selection	55
56	4.3.1	Jets and b tagging	55
57	4.3.2	Lepton selection	56
58	4.3.3	Lepton selection efficiency	57
59	4.4	Background predictions	58
60	4.5	Signal discrimination	59
61	4.5.1	Classifiers response	63
62	4.6	Additional discriminating variables	66

63	5 The CMS forward pixel detector	69
64	5.0.1 The phase 1 FPix upgrade	69
65	5.0.2 FPix module production line	69
66	5.0.3 The Gluing stage	69
67	5.0.4 The Encapsulation stage	69
68	5.0.5 The FPix module production yields	69
69	Bibliography	69
70	References	70

⁷¹ List of Figures

72	1.1	^{14}N neutron capture in a PECVD polymerized pyridine film. The Q-value of this reaction is 626 keV. Taken from [22]	1
74	2.1	Standard model of particle physics.	5
75	2.2	WI transformations between quarks	12
76	2.3	Fundamental interactions in nature.	13
77	2.4	SM interactions diagrams	15
78	2.5	Neutral current processes	21
79	2.6	Spontaneous symmetry breaking mechanism	28
80	2.7	SSB Potential form	29
81	2.8	Potential for complex scalar field	30
82	2.9	SSB mechanism for complex scalar field	31
83	2.10	Higgs production mechanism Feynman diagrams	38
84	2.11	Higgs production cross section and decay branching ratios	39
85	3.1	ref. C.Lefevre, “The CERN accelerator complex,” (2008). CERN-DI- 0812015.	44

87	3.2	ref. J.-L. Caron , “Layout of the LEP tunnel including future LHC in-	
88		frastructures.. L’ensemble du tunnel LEP avec les futures infrastructures	
89		LHC!”, https://cds.cern.ch/record/841542 (Nov, 1993). AC Collection.	
90		Legacy of AC. Pictures from 1992 to 2002..	45
91	3.3	ref. ACTeam, “Diagram of an LHC dipole magnet. Schéma d’un aimant	
92		dipôle du LHC,” (1999). CERN-DI-9906025.	46
93	3.4	ref: CMS Collaboration, “Detector Drawings”, CMS-PHO-GEN-2012-002,	
94		http://cds.cern.ch/record/1433717 , 2012.	48
95	4.1	The two leading-order diagrams of tHq production.	50
96	4.2	Input variables to the BDT for signal discrimination normalized.	60
97	4.3	Input variables to the BDT for signal discrimination not normalized. . .	62
98	4.4	BDT inputs as seen by TMVA against $t\bar{t}$	63
99	4.5	BDT inputs as seen by TMVA against $t\bar{t}V$	64
100	4.6	Correlation matrices for the input variables in the TMVA.	65
101	4.7	MVA classifiers performance.	65
102	4.8	Additional discriminating variables distributions.	67

¹⁰³ List of Tables

104	2.1	Fermions of the SM.	7
105	2.2	Leptons properties.	9
106	2.3	Quarks properties.	10
107	2.4	Fermion weak isospin and weak hypercharge multiplets.	11
108	2.5	Fundamental interactions features.	16
109	2.6	SM gauge bosons.	20
110	2.7	Higgs boson properties.	36
111	2.8	Predicted branching ratios for a SM Higgs boson with $m_H = 125 \text{ GeV}/c^2$.	40
112	4.1	Signal samples and their cross section and branching fraction.	51
113	4.2	κ_V and κ_t combinations.	52
114	4.3	List of background samples used in this analysis (CMSSW 80X).	53
115	4.4	Leading-order $t\bar{t}W$ and $t\bar{t}Z$ samples used in the signal BDT training.	53
116	4.5	Table of high-level triggers that we consider in the analysis.	54
117	4.6	Trigger efficiency scale factors and associated uncertainties.	55
118	4.7	Requirements on each of the three muon selections.	56
119	4.8	Criteria for each of the three electron selections.	57
120	4.9	MVA input discriminating variables	61
121	4.10	TMVA input variables ranking for BDTA_GRAD method	66

122	4.11 TMVA configuration used in the BDT training.	66
123	4.12 ROC-integral for all the testing cases.	68

¹²⁴ Chapter 1

¹²⁵ INTRODUCTION

Figure 1.1: ^{14}N neutron capture in a PECVD polymerized pyridine film. The Q-value of this reaction is 626 keV. Taken from [22]

¹²⁶ **Chapter 2**

¹²⁷ **Theoretical approach**

¹²⁸ **2.1 Introduction**

129 The physical description of the universe is a challenge that physicists have faced by
130 making theories that refine existing principles and proposing new ones in an attempt
131 to embrace emerging facts and phenomena. By early 1800's, there were separate
132 theories describing electric and magnetic phenomena, gravitational force and light.
133 The invention of the electric battery by Alessandro Volta in 1800, the discovery
134 of the magnetic effects of the electric current by Oersted and Ampere (1820), and
135 the generation of electric current using changing magnetic fields by Faraday (1831)
136 represent the first steps in the way to create a unified theory of electromagnetism [1].
137 The unification was carried out by James Clerk Maxwell who was able to merge
138 electricity and magnetism in a set of 20 equations known as "general equations of the
139 electromagnetic field," relating the observables that describe the experimental laws of
140 the electromagnetism. By combining these equations, Maxwell found a wave equation
141 and propose the existence of the "electromagnetic waves." The predicted propagation
142 speed of the electromagnetic waves turned out to be the same as the speed of light,

143 therefore, the natural conclusion was that light is an electromagnetic wave [4]. By
144 1900, waves were considered a perturbation of a material medium which in the case
145 of the electromagnetic waves was identified as the “*Luminiferous Ether*”.

146 By 1900, Max Planck came out with the idea that radiation is quantized [5] and Albert
147 Einstein in 1905 made use of that hypothesis to propose the existence of the light
148 quantum, the “*photon*”, in order to explain the photoelectric effect [6]. The well-
149 known quantum revolution in physics started and the idea of particle-wave duality
150 of photons as a natural behavior was developed and later extended to electrons and
151 to all kind of particles in nature. The development of a quantum theory allowed
152 to predict a set of non-common sense effects like the quantum tunneling and quan-
153 tum entanglement, however, quantum theory was separated from the recently unified
154 electromagnetism.

155 In 1905, Einstein also published two more papers; one aimed to describe his statistical
156 molecular theory of liquids and how it can be used to describe Brownian motion [7].
157 At that time the existence of the atoms and molecules were not fully demonstrated
158 but Einstein’s theory provided an explanation as well as predictions based on the
159 their existence. Jean Perrin in 1908 conducted experiments that confirmed Einstein’s
160 predictions. The other paper described the relationship between space and time [8],
161 unifying the notion of space and time into one entity known as “*spacetime*” that treats
162 space and time at the same level and then discards the absoluteness of time. The
163 new theory known as special relativity, supersedes the Galilean relativity principle
164 and postulates exceptional effects like the time dilation, length contraction and mass-
165 energy equivalence through the most famous formula in physics [9]

$$E = mc^2. \quad (2.1)$$

166 Generalization of the special relativity was presented in 1916 and includes a gener-
 167 alization of Newton’s law of universal gravitation, becoming a unified description of
 168 gravity as a geometric property of space and time. Einstein’s predictions include the
 169 existence of black holes and the recently observed “*gravitational waves*” [10].
 170 At the end of 1940s Julian Schwinger [11] and Richard P. Feynman [12], based in
 171 the work of Sin-Itiro Tomonaga [13], developed an electromagnetic theory consistent
 172 with special relativity and quantum mechanics that describes how matter and light
 173 interact; so-called “quantum eletrodynamics” (QED) had born.
 174 QED has become the guide in the development of theories that describe the universe.
 175 It was the first example of a quantum field theory (QFT), which is the theoretical
 176 framework for building quantum mechanical models that describes particles and their
 177 interactions. QFT is composed of a set of mathematical tools that combines classical
 178 fields, special relativity, and quantum mechanics while keeping the quantum point
 179 particles and locality ideas. This chapter gives an overview of the SM, starting with
 180 the SM particle content, followed by a description of the electroweak interaction,
 181 the Higgs boson and the associated production of Higgs boson and a single top quark
 182 (tH). The description contained in this chapter is based on references ?? unless explicit
 183 reference is provided.

184 **2.2 Standard model of particle physics**

185 Particle physics at the fundamental level is modeled in terms of a collection of in-
 186 teracting particles and fields in a theory known as the “standard model of particle
 187 physics (SM)”¹.

1 The formal and complete treatment of the SM is out of the scope of this document, however a plenty of textbooks describing it at several levels are available in the literature. The treatment in “An Introduction To Quantum Field Theory (Frontiers in Physics)” by Michael E. Peskin

The full picture of the SM is composed of three fields², whose excitations are interpreted as particles called mediators or force-carriers; a set of fields, whose excitations are interpreted as elementary particles, interacting through the exchange of those mediators and a field that give the mass to elementary particles. Figure 2.1 shows a scheme of the SM particles organization. In addition to the particles in the scheme, their corresponding anti-particles, with opposite quantum numbers, are also part of the picture; some particles are their own anti-particles, like photon or Higgs, or anti-particle is already listed like in the W^+ and W^- case.

Standard Model of Elementary Particles

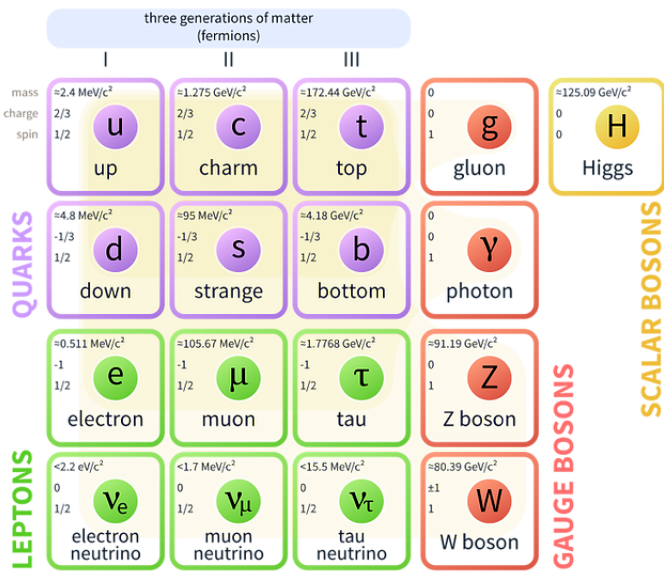


Figure 2.1: Schematic representation of the Standard model of particle physics. SM is a theoretical model intended to describe three of the four fundamental forces of the universe in terms of a set of particles and their interactions. [18].

196 The mathematical formulation of the SM is based on group theory and the use of
 197 Noether's theorem [17] which states that for a physical system modeled by a La-
 198 grangian that is invariant under a group of transformations a conservation law is

and Dan V. Schroeder is quite comprehensive and detailed.

² Note that gravitational field is not included in the standard model formulation

199 expected. For instance, a system described by a time-independent Lagrangian is
 200 invariant (symmetric) under time changes (transformations) with the total energy
 201 conservation law as the expected conservation law. In QED, the Q operator is the
 202 generator of the $U(1)$ symmetry which according to the Noether's theorem means
 203 that there is a conserved charge; this conserved charge is the electric charge and thus
 204 the law conservation of electric charge is established.

205 In the SM, the symmetry group $SU(3)_C \otimes SU(2)_L \otimes U(1)_Y$ describes three of the
 206 four fundamental interactions in nature(see section 2.2.2): strong interaction(SI),
 207 weak interaction(WI) and electromagnetic interactions (EI) in terms of symmetries
 208 associated to physical quantities:

- 209 • Strong: $SU(3)_C$ associated to color charge
- 210 • Weak: $SU(2)_L$ associated to weak isospin and chirality
- 211 • Electromagnetic: $U(1)_Y$ associated to weak hypercharge and electric charge

212 It will be shown that the electromagnetic and weak interactions are combined in
 213 the so-called electroweak interaction where chirality, hypercharge, weak isospin and
 214 electric charge are the central concepts.

215 2.2.1 Fermions

216 The basic constituents of the ordinary matter at the lowest level, which form the
 217 set of elementary particles in the SM formulation, are quarks and leptons. All of
 218 them have spin $1/2$, therefore they are classified as fermions since they obey Fermi-
 219 Dirac statistics. In both cases, they come in six “flavors” and are organized in three
 220 generations, or families, as shown in table 2.1.

221 There is a mass hierarchy between generations where the higher generation particles
 222 decays to the lower one which can explain why the ordinary matter is made of particles
 223 in the first generation. In the SM, neutrinos are modeled as massless particles so they
 224 are not subject to this mass hierarchy; however, today it is known that neutrinos are
 225 massive so the hierarchy could be restated. The reason behind this mass hierarchy is
 226 one of the most important open questions in particle physics, and it becomes more
 227 puzzling when noticing that the mass difference between first and second generation
 228 fermions is small compared to the mass difference with respect to the third generation.
 229 Usually, the second and third generation fermions are produced in high energy pro-
 230 cesses, like the ones recreated in the particle accelerators.

Generation				
	Type	1st	2nd	3rd
Leptons	Charged	Electron (e)	Moun(μ)	Tau (τ)
	Neutral	Electron neutrino (ν_e)	Muon neutrino (ν_μ)	Tau neutrino (ν_τ)
Quarks	Up-type	Up (u)	Charm (c)	Top (t)
	Down-type	Down (d)	Starnge (s)	Bottom (b)

Table 2.1: Fermions of the SM. Quarks and leptons comes in six flavors each and are organized in three generations or families composed of two pairs of closely related particles. The close relationship is motivated by the fact that WI between leptons is limited to the members of the same generation. Generations differs by mass in a way that have been interpreted as a masss hierarchy.

231

232 2.2.1.1 Leptons

233 A lepton is an elementary particle that is not subject to the SI. As seen in table 2.1,
 234 there are two types of leptons, the charged ones (electron, muon and tau) and the
 235 neutral ones (the three neutrinos). The electric charge (Q) is the property that gives
 236 leptons the ability to participate in the EI. From the classical point of view, Q plays
 237 a central role determining, among others, the strength of the electric field through

238 which the electromagnetic force is exerted. It is clear that neutrinos are not affected
 239 by EI because they don't carry electric charge.

240 Another feature of the leptons that is fundamental in the mathematical description
 241 of the SM is the chirality, which is closely related to spin and helicity. Helicity
 242 define the handedness of a particle by relating its spin and momentum such that
 243 if they are parallel then the particle is right-handed; if spin and momentum are
 244 antiparallel the particle is said to be left-handed. The study of parity conservation
 245 (or violation) in β -decay have shown that only left-handed electrons/neutrinos or
 246 right-handed positrons/anti-neutrinos are created [19]; the inclusion of that feature
 247 in the theory was reached by using projection operators for helicity, however, helicity is
 248 frame dependent for massive particles which makes it not Lorentz invariant and then
 249 another related attribute has to be used: *chirality*. Chirality is a purely quantum
 250 attribute which makes it not so easy to describe in graphical terms but it defines
 251 how the wave function of a particle transforms under certain rotations. As with
 252 helicity, there are two chiral states, left-handed chiral (L) and right-handed chiral
 253 (R). In the highly relativistic limit where $E \approx p \gg m$ helicity and chirality converge,
 254 becoming exactly the same for massless particles. In the following when referring
 255 to left-handed (right-handed) it means left-handed chiral (right-handed chiral). The
 256 fundamental fact about chirality is that while EI and SI are not sensitive to chirality,
 257 in WI left-handed and right-handed fermions are treated asymmetrically, such that
 258 only left handed fermions and right-handed anti-fermions are allowed to couple to WI
 259 mediators, which is a violation of parity. The way to translate this statement in a
 260 formal mathematical formulation is based on the isospin symmetry group $SU(2)_L$.
 261 Each generation of leptons is seen as a weak isospin doublet.³ The left-handed charged

³ The weak isospin is an analogy of the isospin symmetry in strong interaction where neutron and proton are affected equally by strong force but differ in its charge.

262 lepton and its associated left-handed neutrino are arranged in doublets of weak isospin
 263 $T=1/2$ while their right-handed partners are singlets:

$$\begin{pmatrix} \nu_l \\ l \end{pmatrix}_L, l_R := \begin{pmatrix} \nu_e \\ e \end{pmatrix}_L, \begin{pmatrix} \nu_\mu \\ \mu \end{pmatrix}_L, \begin{pmatrix} \nu_\tau \\ \tau \end{pmatrix}_L, e_R, \mu_R, \tau_R, \nu_{eR}, \nu_{\mu R}, \nu_{\tau R} \quad (2.2)$$

264 The isospin third component refers to the eigenvalues of the weak isospin operator
 265 which for doublets is $T_3 = \pm 1/2$, while for singlets it is $T_3 = 0$. The physical meaning
 266 of this doublet-singlet arrangement falls in that the WI couples the two particles in
 267 the doublet by exchanging the interaction mediator while the singlet member is not
 268 involved in WI. The main properties of the leptons are summarized in table 2.2.
 269 Altough all three flavor neutrinos have been observed, their masses remain unknown
 270 and only some estimations have been made [20]. The main reason is that the fla-
 271 vor eigenstates are not the same as the mass eigenstates which imply that when a
 272 neutrino is created its mass state is a linear combination of the three mass eigen-
 273 states and experiments can only probe the squared difference of the masses. The
 274 Pontecorvo-Maki-Nakagawa-Sakata (PMNS) mixing matrix encode the relationship
 275 between flavor and mass eigenstates.

Lepton	Q(e)	T_3	L_e	L_μ	L_τ	Mass (MeV/c ²)	Lifetime (s)
Electron (e)	-1	-1/2	1	0	0	0.5109989461(31)	Stable
Electron neutrino(ν_e)	0	1/2	1	0	0	Unknown	Unknown
Muon (μ)	-1	-1/2	0	1	0	105.6583745(24)	$2.1969811(22) \times 10^{-6}$
Muon neutrino (ν_μ)	0	1/2	0	1	0	Unknown	Unknown
Tau (τ)	-1	-1/2	0	0	1	1776.86(12)	$290.3(5) \times 10^{-15}$
Tau neutrino (τ_μ)	0	1/2	0	0	1	Unknown	Unknown

Table 2.2: Leptons properties [21]. Q: electric charge, T_3 : weak isospin. Only left-handed leptons and right-handed anti-leptons participate in the WI. Anti-particles with inverted T_3 , Q and lepton number complete the leptons set but are not listed. Right-handed leptons and left-handed anti-leptons, neither listed, form weak isospin singlets with $T_3 = 0$ and do not take part in the weak interaction.

277 **2.2.1.2 Quarks**

278 Quarks are the basic constituents of protons, neutrons and other non-elementary
 279 particles. The way quarks join to form bound states, called “hadrons”, is through
 280 the SI. Quarks are affected by all the fundamental interactions which means that
 281 they carry all the four types of charges: color, electric charge, weak isospin and mass.
 282 Table 2.3 summarizes the features of quarks, among which the most particular is
 283 their fractional electric charge. Note that fractional charge is not a problem, given
 284 that quarks are not found isolated, but serves to explain how composed particles are
 285 formed out of two or more valence quarks⁴.

Flavor	$Q(e)$	I_3	T_3	B	C	S	T	B'	Y	Color	Mass (MeV/c ²)
Up (u)	2/3	1/2	1/2	1/3	0	0	0	0	1/3	r,b,g	$2.2^{+0.6}_{-0.4}$
Charm (c)	2/3	0	1/2	1/3	1	0	0	0	4/3	r,b,g	$1.28 \pm 0.03 \times 10^3$
Top(t)	2/3	0	1/2	1/3	0	0	1	0	4/3	r,b,g	$173.1 \pm 0.6 \times 10^3$
Down(d)	-1/3	-1/2	-1/2	1/3	0	0	0	0	1/3	r,b,g	$4.7^{+0.5}_{-0.4}$
Strange(s)	-1/3	0	-1/2	1/3	0	-1	0	0	-2/3	r,b,g	96^{+8}_{-4}
Bottom(b)	-1/3	0	-1/2	1/3	0	0	0	-1	-2/3	r,b,g	$4.18^{+0.04}_{-0.03} \times 10^3$

Table 2.3: Quarks properties [21]. Q: electric charge, I_3 : isospin, T_3 : weak isospin, B: baryon number, C: charmness, S: strangeness, T: topness, B' : bottomness, Y: hypercharge. Anti-quarks posses the same mass and spin as quarks but all charges (color, flavor numbers) have opposite sign.

286

287 Color charge is the responsible for the SI between quarks and is the symmetry
 288 ($SU(3)_C$) that defines the formalism to describe SI. There are three colors: red (r),
 289 blue(b) and green(g) and their corresponding three anti-colors; thus each quark carries
 290 one color unit while anti-quarks carries one anti-color unit. As said above, quarks are
 291 not allowed to be isolated due to the color confinement effect, therefore their features
 292 have been studied indirectly by observing their bound states created when:

⁴ Hadrons can contain an indefinite number of virtual quarks and gluons, known as the quark and gluon sea, but only the valence quarks determine hadrons' quantum numbers.

- 293 • one quark with a color charge is attracted by an anti-quark with the correspond-
 294 ing anti-color charge forming a colorless particle called a “meson.”
- 295 • three quarks (anti-quarks) with different color (anti-color) charges are attracted
 296 among them forming a colorless particle called a “baryon(anti-baryon).”
- 297 In the first version of the quark model (1964), M. Gell-Mann [22] and G. Zweig [23,24]
 298 developed a consistent way to classify hadrons according to their properties. Only
 299 three quarks (u, d, s) were involved in a scheme in which all baryons have baryon
 300 number $B=1$ and therefore quarks have $B=1/3$; non-baryons have $B=0$. The scheme
 301 organize baryons in a two-dimensional space (I_3 - Y); Y (hypercharge) and I_3 (isospin)
 302 are quantum numbers related by the Gell-Mann-Nishijima formula [25,26]:

$$Q = I_3 + \frac{Y}{2} \quad (2.3)$$

303 where $Y = B + S + C + T + B'$ are the quantum numbers listed in table 2.3. Baryon
 304 number is conserved in SI and EI which means that single quarks cannot be created
 305 but in pairs $q - \bar{q}$.
 306 Similar to leptons, there are six quark flavors organized in three generations (see table
 307 2.1) and follow a mass hierarchy which again implies that higher generations decay
 308 to first generation quarks.

	Quarks			T_3	Y_W	Leptons			T_3	Y_W
Doublets	$(\begin{smallmatrix} u \\ d' \end{smallmatrix})_L$	$(\begin{smallmatrix} c \\ s' \end{smallmatrix})_L$	$(\begin{smallmatrix} t \\ b' \end{smallmatrix})_L$	$(\begin{smallmatrix} 1/2 \\ -1/2 \end{smallmatrix})$	1/3	$(\begin{smallmatrix} \nu_e \\ e \end{smallmatrix})_L$	$(\begin{smallmatrix} \nu_\mu \\ \mu \end{smallmatrix})_L$	$(\begin{smallmatrix} \nu_\tau \\ \tau \end{smallmatrix})_L$	$(\begin{smallmatrix} 1/2 \\ -1/2 \end{smallmatrix})$	-1
Singlets	u_R	c_R	t_R	0	4/3	ν_{eR}	$\nu_{\mu R}$	$\nu_{\tau R}$	0	-2

Table 2.4: Fermion weak isospin and weak hypercharge multiplets. Weak hypercharge is calculated through the Gell-Mann-Nishijima formula 2.3 but using the weak isospin and charge for quarks.

310 Isospin doublets of quarks are also defined (see table 2.4) and as for neutrinos, the
 311 mass eigenstates are not the same as the WI eigenstates which means that members of
 312 different quark generations are connected by the WI mediator; thus, up-type quarks
 313 are coupled not to down-type quarks directly but to a superposition of down-type
 314 quarks (q'_d) via WI according to:

$$315 \quad q'_d = V_{CKM} q_d$$

$$\begin{pmatrix} d' \\ s' \\ b' \end{pmatrix} = \begin{pmatrix} V_{ud} & V_{us} & V_{ub} \\ V_{cd} & V_{cs} & V_{cb} \\ V_{td} & V_{ts} & V_{tb} \end{pmatrix} \begin{pmatrix} d \\ s \\ b \end{pmatrix} \quad (2.4)$$

316 where V_{CKM} is known as Cabibbo-Kobayashi-Maskawa (CKM) mixing matrix [27,28].

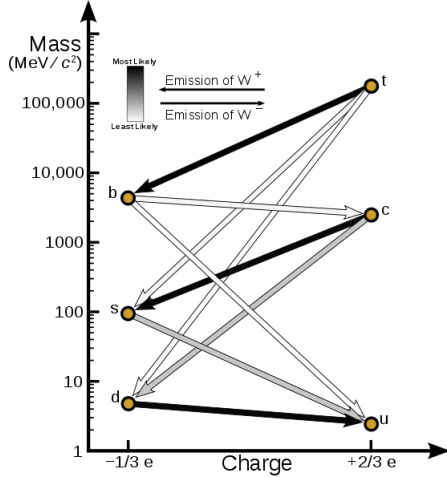


Figure 2.2: Transformations between quarks through WI. Higher generations quarks decay to first generation quarks by emitting a W boson. The arrow color indicates the likelihood of the transition according to the grey scale in the top left side which represent the CKM matrix parameters [29].

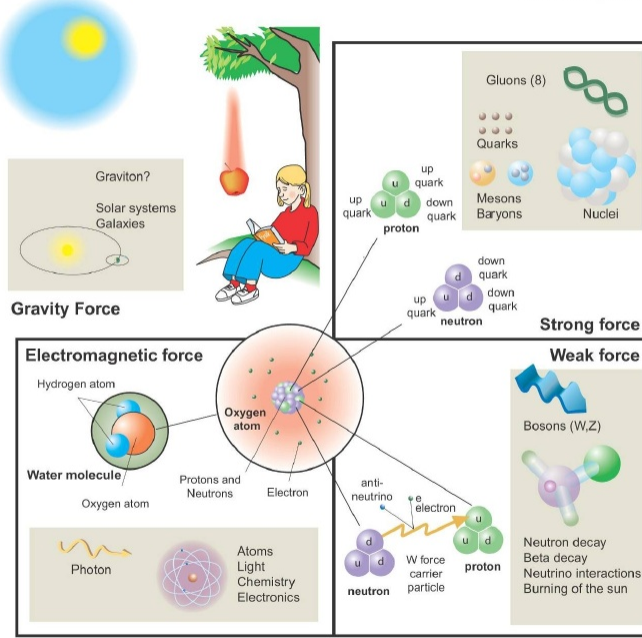
317 The weak decays of quarks are represented in the diagram of figure 2.2; again the CKM
 318 matrix plays a central role since it contains the probabilities for the different quark
 319 decay channels, in particular, note that quark decays are greatly favored between

320 generation members.
 321 CKM matrix is a 3×3 unitary matrix parametrized by three mixing angles and the
 322 *CP-mixing phase*; the latter is the parameter responsible for the CP-violation in the
 323 SM. The fact that the b quark decays almost all the times to a top quark is exploited
 324 in this thesis when making the selection of the signal events by requiring the presence
 325 of a jet tagged as a jet coming from a b quark in the final state. The effect of the
 326 *CP-mixing phase* on the cross section of associated production of Higgs boson and a
 327 single top process is also explored in this thesis.

328 2.2.2 Fundamental interactions

Fundamental interactions.

Illustration: Typoform



Summer School KPI 15 August 2009

Figure 2.3: Fundamental interactions in nature. Despite the many manifestations of forces in nature, we can track all of them back to one of the fundamental interactions. The most common forces are gravity and electromagnetic given that all of us are subject and experience them in everyday life.

329 Even though there are many manifestations of force in nature, like the ones represented
 330 in figure 2.3, we can classify all of them into one of four fundamental interactions:
 331

- 332 ● *Electromagnetic interaction (EI)* affect particles that are “electrically charged,”
 333 like electrons and protons. It is described by QED combining quantum mechanics,
 334 special relativity and electromagnetism in order to explain how particles
 335 with electric charge interact through the exchange of photons, therefore, one
 336 says that “Electromagnetic Force” is mediated by “photons”. Figure 2.4a) shows
 337 a graphical representation, known as “feynman diagram”, of electron-electron
 338 scattering.
- 339 ● *Strong interaction (SI)* described by Quantum Chromodynamics (QCD). Hadrons
 340 like proton and neutron have internal structure given that they are composed
 341 of two or more valence quarks⁵. Quarks have fractional electric charge which
 342 means that they are subject to electromagnetic interaction and in the case of the
 343 proton they should break apart due to electrostatic repulsion; however, quarks
 344 are held together inside the hadrons against their electrostatic repulsion by the
 345 “Strong Force” through the exchange of “gluons.” The analog to the electric
 346 charge is the “color charge”. Electrons and photons are elementary particles
 347 as quarks but they don’t carry color charge, therefore they are not subject to
 348 SI. The feynman diagram for gluon exchange between quarks is shown in figure
 349 2.4b).
- 350 ● *Weak interaction (WI)* described by the Weak theory (WT), is responsible for
 351 instance for the radioactive decay in atoms and proton-proton (pp) fusion within
 352 the sun. Quarks and leptons are the particles affected by the weak interaction

⁵ particles made of four and five quarks are exotic states not so common

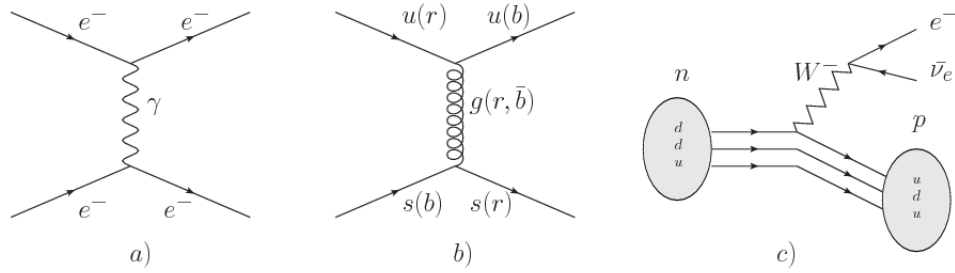


Figure 2.4: Feynman diagrams representing the interactions in SM; a) EI: e - e scattering; b) SI: gluon exchange between quarks ; c) WI: β -decay

and posses a property called “flavor charge” which can be changed by emitting or absorbing one weak force mediator; they comes in six flavors each (see 2.2.1). There are three mediators of the “Weak force” known as “Z” boson in the case of electrically neutral changes and “ W^\pm ” bosons in the case of electrically charged changes. The “weak isospin” is the WI analog to electric charge in EI and color charge in SI and define how quarks and leptons are affected by the weak force. Figure 2.4c) shows the feynman diagram of β -decay where a newtron (n) is transformed in a proton (p) by emmiting a W^- particle. Since this thesis is in the frame of the electroweak interaction, a more detailed description of it will be given in section 2.3

- *Gravitational interaction (GI)* described by General Theory of Relativity (GR). It is responsible for the structure of galaxies and black holes as well as the expansion of the universe. As a classical theory, in the sense that it can be formulated without even appeal to the concept of quantization, it implies that the spacetime is a continuum and predictions can be made without limitation to the precision of the measurement tools which represent a direct contradiction of the quantum mechanics principles. Gravity is deterministic while quantum mechanics is probabilistic; despite that, efforts to develop a quantum theory of

371 gravity have predicted the “graviton” as mediator of the Gravitational force⁶.

Interaction	Acts on	Relative strength	Range (m)	Mediators
Electromagnetic (QED)	Electrically charged particles	10^{-2}	Infinite	Photon
Strong (QCD)	Quarks and gluons	1	10^{-15}	Gluon
Weak (WI)	Leptons and quarks	10^{-6}	10^{-18}	W^\pm, Z
Gravitational (GI)	Massive particles	10^{-39}	Infinite	Graviton

Table 2.5: Fundamental interactions features [30].

372

373 Table 2.5 summarizes the main features of the fundamental interactions. The relative
 374 strength of the fundamental forces reveals the meaning of strong and weak; in a
 375 context where the relative strength of the SI is 1, the EI is about hundred times
 376 weaker and WI is about million times weaker than the SI. A good description on
 377 how the relative strength and range of the fundamental interactions are calculated
 378 can be found in references [30, 31]. In the everyday life, only EI and GI are explicitly
 379 experienced due to the range of these interactions; i.e., at the human scale distances
 380 only EI and GI have appreciable effects, in contrast to SI which at distances greater
 381 than 10^{-15} m become negligible.

382 QED was built successfully on the basis of the classical electrodynamics theory of
 383 Maxwell and Lorentz (CED), following theoretical and experimental requirements
 384 imposed by

- 385 • lorentz invariance: independence on the reference frame.
 386 • locality: interacting fields are evaluated at the same space-time point to avoid
 387 action at a distance.

⁶ Actually a wide variety of theories have been developed in an attempt to describe gravity; some famous examples are string theory and supergravity.

- 388 • renormalizability: physical predictions are finite and well defined
- 389 • particle spectrum, symmetries and conservation laws already known must emerge
- 390 from the theory.
- 391 • gauge invariance.
- 392 The gauge invariance requirement reflects the fact that the fundamental fields cannot
- 393 be directly measured but associated fields which are the observables. Electric (“**E**”)
- 394 and magnetic (“**B**”) fields in CED are associated with the electric scalar potential
- 395 “V” and the vector potential “**A**”. In particular, **E** can be obtained by measuring
- 396 the change in the space of the scalar potential (ΔV); however, two scalar potentials
- 397 differing by a constant “f” correspond to the same electric field. The same happens
- 398 in the case of the vector potential “**A**”; thus, different configurations of the associated
- 399 fields result in the same set of values of the observables. The freedom in choosing
- 400 one particular configuration is known as “gauge freedom”; the transformation law
- 401 connecting two configurations is known as “gauge transformation” and the fact that
- 402 the observables are not affected by a gauge transformation is called “gauge invariance”.
- 403 When the gauge transformation:

$$\begin{aligned} \mathbf{A} &\rightarrow \mathbf{A} - \nabla f \\ V &\rightarrow V - \frac{\partial f}{\partial t} \end{aligned} \tag{2.5}$$

- 404 is applied to Maxwell equations, they are still satisfied and the fields remain invariant.
- 405 Thus, the classical electrodynamics theory is invariant under gauge transformations
- 406 and is called a “gauge theory”. The set of all gauge transformations form the “sym-
- 407 metry group” of the theory, which according to the group theory, has a set of “group

408 generators". The number of group generators determine the number of "gauge fields"
 409 of the theory.

410 As mentioned in the first lines of section 2.2, QED has one symmetry group ($U(1)$)
 411 with one group generator (the Q operator) and one gauge field (the electromagnetic
 412 field A^μ). In CED there is not a clear definition, beyond the historical convention, of
 413 which fields are the fundamental and which are the associated, but in QED it is clear
 414 that the fundamental field is A^μ . When a gauge theory is quantized, the gauge field
 415 is quantized and its quanta is called "gauge boson". The word boson characterize
 416 particles with integer spin which obvey Bose-einstein statistics.

417 As will be detailed in section 2.3, interactions between particles in a system can be
 418 obtained by considering first the Lagrangian density of free particles in the system,
 419 which of course is incomplete because the interaction terms have been left out, and
 420 demanding global phase transformation invariance. Global phase transformation in-
 421 variance means that a gauge transformation is performed identically to every point in
 422 the space⁷ and the Lagrangian remains invariant. Then, the global transformation is
 423 promoted to a local phase transformation (this time the gauge transformation depends
 424 on the position in space) and again invariance is required. Due to the space depen-
 425 dence of the local tranformation, the Lagrangian density is not invariant anymore.

426 In order to restate the gauge invariance, the gauge covariant derivative is introduced
 427 in the Lagrangian and with it the gauge field responsible for the interaction between
 428 particles in the system. The new Lagrangian density is gauge invariant, includes the
 429 interaction terms needed to account for the interactions and provide a way to explain
 430 the interaction between particles through the exchange of the gauge boson.

431 This recipe was used to build QED and the theories that aim to explain the funda-
 432 mental interactions.

⁷ Here space corresponds to the 4-dimensional space i.e. space-time.

433 **2.2.3 Gauge Bosons**

434 The importance of the gauge bosons comes from the fact that they are the force
 435 mediators or force carriers. The features of the gauge bosons reflect the features of
 436 the fields they represent; these fetures are extracted from the Lagrangian density used
 437 to describe the interactions. In section 2.3, it will be shown how the gauge bosons
 438 of the EI and WI emerge from the electrowaek Lagrangian. The SI gauge bosons
 439 features are also extracted from the SI Lagrangian but it is not detailed in this
 440 document. Here, the main features of the SM gauge bosons will be briefly presented
 441 and summarized in table 2.6.

442 • **Photon.** EI occurs when the photon couples to (is exchanged between) particles
 443 carrying electric charge; however, the photon itself does not carry electric charge,
 444 therefore, there is no coupling between photons. Given that the photon is
 445 massless the EI is of infinite range i.e. electrically charged particles interact
 446 even if they are located far away one from each other; that also means that
 447 photons always move with the speed of light.

448 • **Gluon.** SI is mediated by gluons, which same as photons are massless. They
 449 carry one unit of color charge and one unit of anticolor charge which means that
 450 gluons couples to other gluons. As a result, the range of the SI is not infinite
 451 but very short due to the attraction between gluons, giving rise to the “color
 452 confinement” which explains why color charged particles cannot be isolated but
 453 live within composited particles, like quarks inside protons.

454 • **W, Z.** The EWI mediators, W^\pm and Z, are massive which explain its short-
 455 range. Given that the WI is the only interaction that can change the flavor
 456 of the interacting particles, the W boson is the responsible for the nuclear

457 transmutation where a neutron is converted in a proton or vice versa with the
 458 involvement of an electron and a neutrino. The Z boson is the responsible of the
 459 neutral weak processes like neutrino elastic scattering where no electric charge
 460 but momentum transference is involved. WI gauge bosons carry isospin charge
 461 which makes possible the interaction between them.

Interaction	Mediator	Electric charge (e)	Color charge	Weak Isospin	mass (GeV/c^2)
Electromagnetic	Photon (γ)	0	No	0	0
Strong	Gluon (g)	0	Yes -octet	No	0
Weak	W^\pm	± 1	No	± 1	80.385 ± 0.015
	Z	0	No	0	91.188 ± 0.002

Table 2.6: SM gauge bosons main features [21].

462

463 2.3 Electroweak unification and the Higgs 464 mechanism

465 Physicist dreams of building a theory that contains all the interactions in one single
 466 interaction, i.e. showing that at some scale in energy all the four fundamental in-
 467 teractions are unified and only one interaction emerges in a “Theory of everything”.
 468 The first sign of the feasibility of such unification comes from success in the con-
 469 struction of the CED. Einstein spent years trying to reach that dream, which by
 470 1920 only involved electromagnetism and gravity, with no success; however, a new
 471 partial unification was achieved in the 1960’s, when S.Glashow [14], A.Salam [15] and
 472 S.Weinberg [16] independently proposed that electromagnetic and weak interactions
 473 are two manifestations of a more general interaction called “electroweak interaction.”
 474 QCD and EWT were developed in parallel and following the useful prescription pro-
 475 vided by QED and the gauge invariance principles.

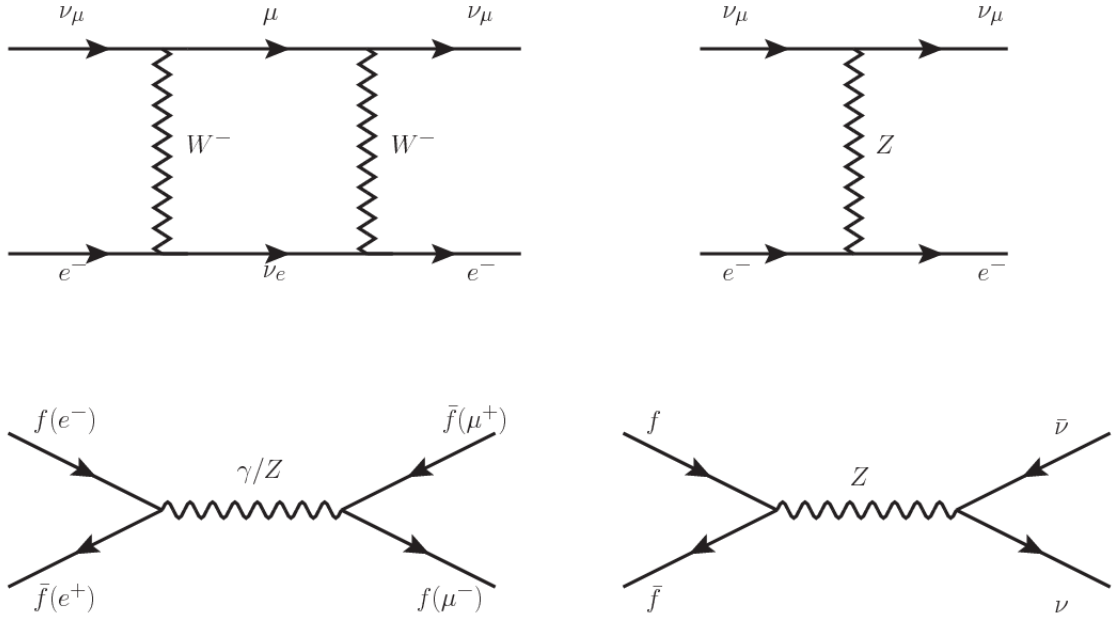


Figure 2.5: Top: $\nu_\mu - e^-$ scattering going through charged currents (left) and neutral currents (right). Bottom: neutral current processes for charged fermions (left) and involving neutrinos (right). While neutral current processes involving only charged fermions can proceed through EI or WI, those involving neutrinos can only proceed via WI.

476 The theory of weak interactions was capable of explaining the β -decay and in general
477 the processes mediated by W^\pm bosons. However, there were some processes like the
478 “ $\nu_\mu - e$ scattering” which would require the exchange of two W bosons (see figure 2.5
479 top diagrams) giving rise to divergent loop integrals and then non finite predictions.
480 By including neutral currents involving fermions via the exchange of neutral bosons
481 Z, those divergences are compensated and the predictions become realistic.
482 Neutral weak interaction vertices conserve flavor in the same way as the electromag-
483 netic vertices do, but additionally, the Z boson can couple to neutrinos which implies
484 that processes involving charged fermions can proceed through EI or WI but processes
485 involving neutrinos can proceed only through WI.
486 The prescription to build a gauge theory of the WI consist of proposing a free field La-
487 grangian density that includes the particles involved; next, by requesting invariance

under global phase transformations first and generalizing to local phase transformations invariance later, the conserved currents are identified and interactions are generated by introducing gauge fields. Given that the goal is to include the EI and WI in a single theory, the group symmetry considered should be a combination of $SU(2)_L$ and $U(1)_{em}$, however the latter cannot be used directly because the EI treat left and right-handed particles indistinctly in contrast to the former. Fortunately, the weak hypercharge, which is a combination of the weak isospin and the electric charge (eqn 2.3) is suitable to be used since it is conserved by the EI and WI. Thus, the symmetry group to be considered is

$$G \equiv SU(2)_L \otimes U(1)_Y \quad (2.6)$$

The following treatment applies to any of the fermion generations but for simplicity the first generation of leptons will be considered [2, 3, 32, 33]. Also, the unified weak and electromagnetic interaction will be referred as “Electroweak Interaction (EWI).”

Given the first generation of leptons

$$\psi_1 = \begin{pmatrix} \nu_e \\ e^- \end{pmatrix}_L, \quad \psi_2 = \nu_{eR}, \quad \psi_3 = e_R^- \quad (2.7)$$

the charged fermionic currents are given by

$$J_\mu \equiv J_\mu^+ = \bar{\nu}_{eL} \gamma_\mu e_L, \quad J_\mu^\dagger \equiv J_\mu^- = \bar{e}_L \gamma_\mu \nu_{eL} \quad (2.8)$$

and the free Lagrangian is given by

$$\mathcal{L}_0 = \sum_{j=1}^3 i\bar{\psi}_j(x) \gamma^\mu \partial_\mu \psi_j(x). \quad (2.9)$$

Mass terms are included directly in the QED and QCD free Lagrangians since they

504 preserve the invariance under the symmetry transformations involved which treat
 505 left-handed and right-handed similarly, however mass terms of the form

$$m_W^2 W_\mu^\dagger(x) W^\mu(x) + \frac{1}{2} m_Z^2 Z_\mu(x) Z^\mu(x) - m_e \bar{\psi}_e(x) \psi_e(x) \quad (2.10)$$

506 which represent the mass of W^\pm , Z and electrons, are not invariant under G trans-
 507 formations, therefore the gauge fields described by the EWI are in principle massless.
 508 Experiments have shown that the gauge fields are not massless; however, they have to
 509 acquire mass through a mechanism compatible with the gauge invariance; that mech-
 510 anism is known as the “Higgs mechanism” and will be considered later in this section.
 511 The global transformations in the combined symmetry group G can be written as

$$\begin{aligned} \psi_1(x) &\xrightarrow{G} \psi'_1(x) \equiv U_Y U_L \psi_1(x), \\ \psi_2(x) &\xrightarrow{G} \psi'_2(x) \equiv U_Y \psi_2(x), \\ \psi_3(x) &\xrightarrow{G} \psi'_3(x) \equiv U_Y \psi_3(x) \end{aligned} \quad (2.11)$$

512 where U_L represent the $SU(2)_L$ transformation acting on the weak isospin doublet
 513 only and U_Y represent the $U(1)_Y$ transformation acting on all the weak isospin mul-
 514 tiplets. Explicitly

$$U_L \equiv \exp\left(i \frac{\sigma_i}{2} \alpha^i\right), \quad U_Y \equiv \exp(i y_i \beta) \quad (i = 1, 2, 3) \quad (2.12)$$

515 with σ_i the Pauli matrices and y_i the weak hypercharges. In order to promote the
 516 transformations from global to local keeping the invariance, it is required that $\alpha^i =$
 517 $\alpha^i(x)$ and $\beta = \beta(x)$ and the replace of the ordinary derivatives by the covariant
 518 derivatives

$$\begin{aligned}
D_\mu \psi_1(x) &\equiv \left[\partial_\mu + ig\sigma_i W_\mu^i(x)/2 + ig'y_1 B_\mu(x) \right] \psi_1(x) \\
D_\mu \psi_2(x) &\equiv \left[\partial_\mu + ig'y_2 B_\mu(x) \right] \psi_2(x) \\
D_\mu \psi_3(x) &\equiv \left[\partial_\mu + ig'y_3 B_\mu(x) \right] \psi_3(x)
\end{aligned} \tag{2.13}$$

519 introducing four gauge fields, $W_\mu^i(x)$ and $B_\mu(x)$, in the process. The covariant deriva-
520 tives (eqn 2.13) are required to transform in the same way as fermion fields $\psi_i(x)$
521 themselves, therefore, the gauge fields transform as:

$$\begin{aligned}
B_\mu(x) &\xrightarrow{G} B'_\mu(x) \equiv B_\mu(x) - \frac{1}{g'} \partial_\mu \beta(x) \\
W_\mu^i(x) &\xrightarrow{G} W_\mu^{i'}(x) \equiv W_\mu^i(x) - \frac{i}{g} \partial_\mu \alpha_i(x) - \varepsilon_{ijk} \alpha_j(x) W_\mu^k(x).
\end{aligned} \tag{2.14}$$

522 The G invariant version of the Lagrangian density 2.9 can be written as

$$\mathcal{L}_0 = \sum_{j=1}^3 i\bar{\psi}_j(x) \gamma^\mu D_\mu \psi_j(x) \tag{2.15}$$

523 where free massless fermion and gauge fields and fermion-gauge boson interactions
524 are included. The EWI Lagrangian density must additionally include kinetic terms
525 for the gauge fields (\mathcal{L}_G) which are built from the field strengths, according to

$$B_{\mu\nu}(x) \equiv \partial_\mu B_\nu - \partial_\nu B_\mu \tag{2.16}$$

$$W_{\mu\nu}^i(x) \equiv \partial_\mu W_\nu^i(x) - \partial_\nu W_\mu^i(x) - g\varepsilon^{ijk} W_\mu^j W_\nu^k \tag{2.17}$$

526 the last term in eqn. 2.17 is added in order to hold the gauge invariance; therefore,

$$\mathcal{L}_G = -\frac{1}{4}B_{\mu\nu}(x)B^{\mu\nu}(x) - \frac{1}{4}W_{\mu\nu}^i(x)W_i^{\mu\nu}(x) \quad (2.18)$$

527 which contains not only the free gauge fields contributions but also the gauge fields
 528 self-interactions and interactions among them.

529 The three weak isospin conserved currents resulting from the $SU(2)_L$ symmetry are
 530 given by

$$J_\mu^i(x) = \frac{1}{2}\bar{\psi}_1(x)\gamma_\mu\sigma^i\psi_1(x) \quad (2.19)$$

531 while the weak hypercharge conserved current resulting from the $U(1)_Y$ symmetry is
 532 given by

$$J_\mu^Y = \sum_{j=1}^3 \bar{\psi}_j(x)\gamma_\mu y_j\psi_j(x) \quad (2.20)$$

533 In order to evaluate the electroweak interactions modeled by an isotriplet fields W_μ^i
 534 which couples to isospin currents J_μ^i with strength g and additionally the singlet
 535 field B_μ which couples to the weak hypercharge current J_μ^Y with strength $g'/2$, the
 536 interaction Lagrangian density to be considered is

$$\mathcal{L}_I = -g J^{i\mu}(x) W_\mu^i(x) - \frac{g'}{2} J^Y{}^\mu(x) B_\mu(x) \quad (2.21)$$

537 Note that the weak isospin currents are not the same as the charged fermionic currents
 538 that were used to describe the WI (eqn 2.8), since the weak isospin eigenstates are
 539 not the same as the mass eigenstates, but they are closely related

$$J_\mu = \frac{1}{2}(J_\mu^1 + iJ_\mu^2), \quad J_\mu^\dagger = \frac{1}{2}(J_\mu^1 - iJ_\mu^2). \quad (2.22)$$

540 The same happen with the gauge fields W_μ^i which are related to the mass eigenstates
 541 W^\pm by

$$W_\mu^+ = \frac{1}{\sqrt{2}}(W_\mu^1 - iW_\mu^2), \quad W_\mu^- = \frac{1}{\sqrt{2}}(W_\mu^1 + iW_\mu^2). \quad (2.23)$$

542 The fact that there are three weak isospin conserved currents is an indication that in
 543 addition to the charged fermionic currents which couple charged to neutral leptons
 544 there should be a neutral fermionic current that couples neutral fermions or electri-
 545 cally charged fermions that has the same electric charge and thus does not imply
 546 electric charge change. The third weak isospin current contains a term that is simi-
 547 lar to the electromagnetic current (j_μ^{em}), indicating that there is a relation between
 548 them and resembling the Gell-Mann-Nishijima formula 2.3 adapted to electroweak
 549 interactions

$$Q = T_3 + \frac{Y_W}{2}. \quad (2.24)$$

550 Just as Q generates the $U(1)_{em}$ symmetry, the weak hypercharge generates the $U(1)_Y$
 551 symmetry as said before. It is possible to write the relationship in terms of the currents
 552 as

$$j_\mu^{em} = J_\mu^3 + \frac{1}{2}J_\mu^Y. \quad (2.25)$$

553 The neutral gauge fields W_μ^3 and B_μ cannot be directly identified with the Z and the
 554 photon fields since the photon interacts similarly with left and right-handed fermions;
 555 however, they are related through a linear combination given by

$$A_\mu = B_\mu \cos \theta_W + W_\mu^3 \sin \theta_W \quad (2.26)$$

$$Z_\mu = -B_\mu \sin \theta_W + W_\mu^3 \cos \theta_W$$

556 where θ_W is known as the “Weinberg angle.” The interaction Lagrangian is now given

557 by

$$\mathcal{L}_I = -\frac{g}{\sqrt{2}}(J^\mu W_\mu^+ + J^{\mu\dagger} W_\mu^-) - \left(g \sin \theta_W J_\mu^3 + g' \cos \theta_W \frac{J_\mu^Y}{2}\right) A^\mu - \left(g \cos \theta_W J_\mu^3 - g' \sin \theta_W \frac{J_\mu^Y}{2}\right) Z^\mu \quad (2.27)$$

558 the first term is the weak charged current interaction, while the second term is the

559 electromagnetic interaction under the condition

$$g \sin \theta_W = g' \cos \theta_W = e, \quad \frac{g'}{g} = \tan \theta_W \quad (2.28)$$

560 contained in the eqn.2.25; the third term is the neutral weak current.

561 Note that the neutral fields transformation given by the eqn. 2.26 can be written in

562 terms of the coupling constants g and g' as:

$$A_\mu = \frac{g' W_\mu^3 + g B_\mu}{\sqrt{g^2 + g'^2}}, \quad Z_\mu = \frac{g W_\mu^3 - g' B_\mu}{\sqrt{g^2 + g'^2}} \quad (2.29)$$

563 So far, the Lagrangian density describing the non-massive EWI is:

$$\mathcal{L}_{nmEWI} = \mathcal{L}_0 + \mathcal{L}_G \quad (2.30)$$

564 where fermion and gauge fields have been considered massless because their regular

565 mass terms are manifestly non invariant under G transformations; therefore, masses

566 have to be generated in a gauge invariant way. The mechanism by which this goal is

567 achieved is known as the “Higgs mechanism” and is closely connected to the concept
 568 of “spontaneous symmetry breaking.”

569 2.3.1 Spontaneous symmetry breaking

570 Figure 2.6 left shows a steel nail (top) which is subject to an external force; the form
 of the potential energy is also shown (bottom).

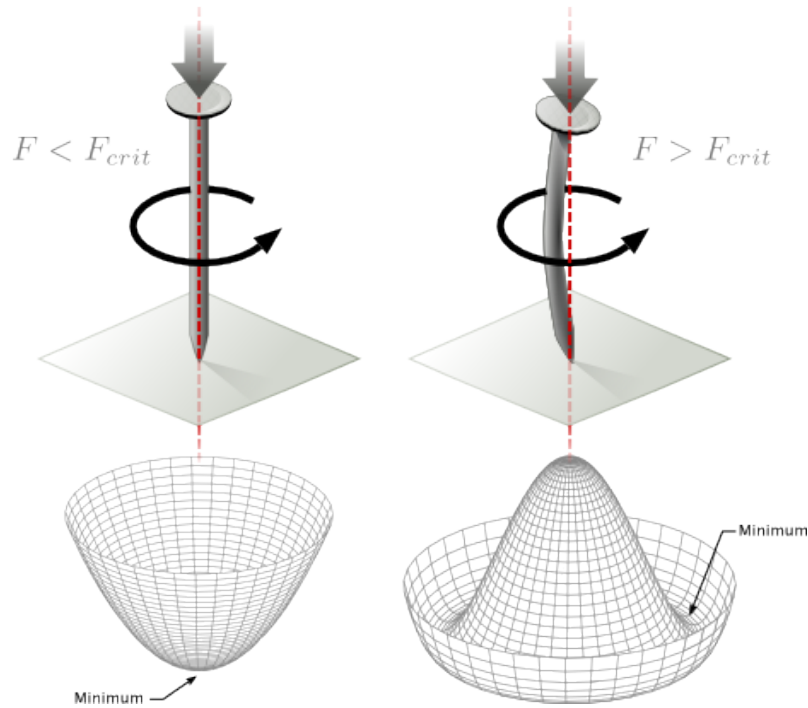


Figure 2.6: Spontaneous symmetry breaking mechanism. The steel nail, subject to an external force (top left), has rotational symmetry with respect to its axis. When the external force overcomes a critical value the nail buckles (top right) choosing a minimal energy state (ground state) and thus “*breaking spontaneously the rotational symmetry*”. The potential energy (bottom) changes but holds the rotational symmetry; however, an infinite number of asymmetric ground states are generated and circularly distributed in the bottom of the potential [34].

571
 572 Before reaching the critical force value, the system has rotational symmetry with re-
 573 spect to the nail axis; however, after the critical force value is reached the nail buckles
 574 (top right). The form of the potential energy (bottom right) changes, preserving its

575 rotational symmetry although its minima do not exhibit that rotational symmetry
 576 any longer. Right before the nail buckles there is no indication of the direction the
 577 nail will bend because any of the directions are equivalent, but once the nail bent,
 578 choosing a direction, an arbitrary minimal energy state (ground state) is selected and
 579 it does not share the system rotational symmetry. This mechanism for reaching an
 580 asymmetric ground state is known as “*spontaneous symmetry breaking (SSB)*”.

581 The lesson from this analysis is that the way to introduce the SSB mechanism into a
 582 system is by adding the appropriate potential to it.

583 Figure 2.7 shows a plot of the potential $V(\phi)$ in the case of a scalar field ϕ

$$V(\phi) = \mu^2 \phi^\dagger \phi + \lambda (\phi^\dagger \phi)^2 \quad (2.31)$$

584 If $\mu^2 > 0$ the potential has only one minimum at $\phi = 0$ and describe a scalar field
 585 with mass μ . If $\mu^2 < 0$ the potential has a local maximum at $\phi = 0$ and two minima
 586 at $\phi = \pm\sqrt{-\mu^2/\lambda}$ which enables the SSB mechanism to work.

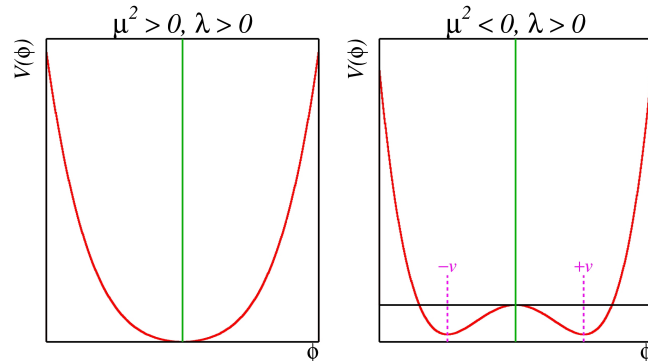


Figure 2.7: Shape of the potential $V(\phi)$ for $\lambda > 0$ and: $\mu^2 > 0$ (left) and $\mu^2 < 0$ (right). The case $\mu^2 < 0$ corresponds to the potential suitable for introducing the SSB mechanism by choosing one of the two ground states which are connected via reflection symmetry. [34].

587 In the case of a complex scalar field $\phi(x)$

$$\phi(x) = \frac{1}{\sqrt{2}}(\phi_1 + i\phi_2) \quad (2.32)$$

588 the Lagrangian (invariant under global $U(1)$ transformations) is given by

$$\mathcal{L} = (\partial_\mu \phi)^\dagger (\partial^\mu \phi) - V(\phi), \quad V(\phi) = \mu^2 \phi^\dagger \phi + \lambda (\phi^\dagger \phi)^2 \quad (2.33)$$

589 where an appropriate potential has been added in order to introduce the SSB.

590 As seen in figure 2.8, the potential has now an infinite number of minima circularly
 591 distributed along the ξ -direction which makes possible the occurrence of the SSB by
 592 choosing an arbitrary ground state; for instance, $\xi = 0$, i.e. $\phi_1 = v, \phi_2 = 0$

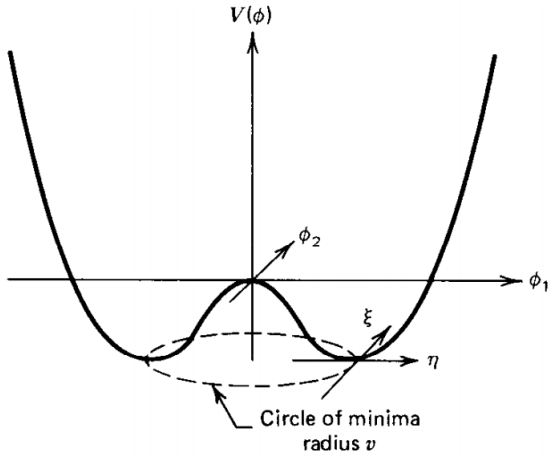


Figure 2.8: Potential for complex scalar field. There is a circle of minima of radius v along the ξ -direction [3].

$$\phi_0 = \frac{v}{\sqrt{2}} \exp(i\xi) \xrightarrow{\text{SSB}} \phi_0 = \frac{v}{\sqrt{2}} \quad (2.34)$$

593 As usual, excitations over the ground state are studied by making an expansion about
 594 it; thus, the excitation can be parametrized as:

$$\phi(x) = \frac{1}{\sqrt{2}}(v + \eta(x) + i\xi(x)) \quad (2.35)$$

595 which when substituted into eqn. 2.33 produces a Lagrangian in terms of the new
 596 fields η and ξ

$$\mathcal{L}' = \frac{1}{2}(\partial_\mu \xi)^2 + \frac{1}{2}(\partial_\mu \eta)^2 + \mu^2 \eta^2 - V(\phi_0) - \lambda v \eta (\eta^2 + \xi^2) - \frac{\lambda}{4}(\eta^2 + \xi^2)^2 \quad (2.36)$$

597 where the last two terms represent the interactions and self-interaction between the
 598 two fields η and ξ . The particular feature of the SSB mechanism is revealed when
 599 looking to the first three terms of \mathcal{L}' . Before the SSB, only the massless ϕ field is
 600 present in the system; after the SSB there are two fields of which the η -field has
 601 acquired mass $m_\eta = \sqrt{-2\mu^2}$ while the ξ -field is still massless (see figure 2.9).

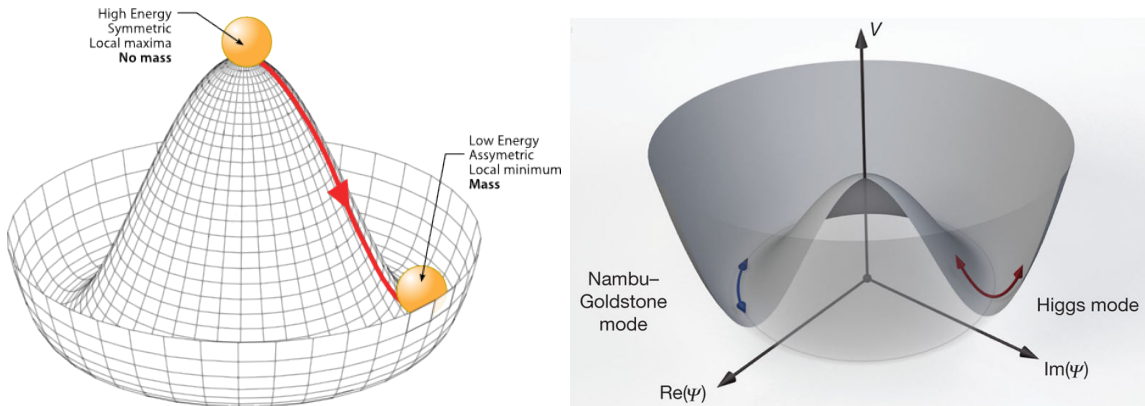


Figure 2.9: SSB mechanism for a complex scalar field [34, 35].

602 Thus, the SSB mechanism serves as a method to generate mass but as a side effect a
 603 massless field is introduced in the system. This fact is known as the Goldstone theorem
 604 and states that a massless scalar field appears in the system for each continuous
 605 symmetry spontaneously broken. Another version of the Goldstone theorem states
 606 that “if a Lagrangian is invariant under a continuous symmetry group G , but the
 607 vacuum is only invariant under a subgroup $H \subset G$, then there must exist as many
 608 massless spin-0 particles (Nambu-Goldstone bosons) as broken generators.” [33] The

609 Nambu-Goldstone boson can be understood considering that the potential in the ξ -
 610 direction is flat so excitations in that direction are not energy consuming and thus
 611 represent a massless state.

612 2.3.2 Higgs mechanism

613 When the SSB mechanism is introduced in the formulation of the EWI in an attempt
 614 to generate the mass of the so far massless gauge bosons and fermions, an interesting
 615 effect is revealed. In order to keep the G symmetry group invariance and generate
 616 the mass of the EW gauge bosons a G invariant Lagrangian density (\mathcal{L}_S) has to be
 617 added to the non massive EWI Lagrangian (eqn. 2.30)

$$\mathcal{L}_S = (D_\mu \phi)^\dagger (D^\mu \phi) - \mu^2 \phi^\dagger \phi - \lambda (\phi^\dagger \phi)^2, \quad \lambda > 0, \mu^2 < 0 \quad (2.37)$$

$$D_\mu \phi = \left(i\partial_\mu - g \frac{\sigma_i}{2} W_\mu^i - g' \frac{Y}{2} B_\mu \right) \phi \quad (2.38)$$

618 ϕ has to be an isospin doublet of complex scalar fields so it preserves the G invariance;
 619 thus ϕ can be defined as:

$$\phi = \begin{pmatrix} \phi^+ \\ \phi^0 \end{pmatrix} \equiv \frac{1}{\sqrt{2}} \begin{pmatrix} \phi_1 + i\phi_2 \\ \phi_3 + i\phi_4 \end{pmatrix}. \quad (2.39)$$

620 The minima of the potential are defined by

$$\phi^\dagger \phi = \frac{1}{2} (\phi_1^2 + \phi_2^2 + \phi_3^2 + \phi_4^2) = -\frac{\mu^2}{2\lambda}. \quad (2.40)$$

621 The choice of the ground state is critical. By choosing a ground state, invariant under
 622 $U(1)_{em}$ gauge symmetry, the photon will remain massless and the W^\pm and Z bosons
 623 masses will be generated which is exactly what is needed. In that sense, the best

624 choice corresponds to a weak isospin doublet with $T_3 = -1/2$, $Y_W = 1$ and $Q = 0$
 625 which defines a ground state with $\phi_1 = \phi_2 = \phi_4$ and $\phi_3 = v$:

$$\phi_0 \equiv \frac{1}{\sqrt{2}} \begin{pmatrix} 0 \\ v \end{pmatrix}, \quad v^2 \equiv -\frac{\mu^2}{\lambda}. \quad (2.41)$$

626 where the vacuum expectation value v is fixed by the Fermi coupling G_F according
 627 to $v = (\sqrt{2}G_F)^{1/2} \approx 246$ GeV.

628 The G symmetry has been broken and three Nambu-Goldstone bosons will appear.
 629 The next step is to expand ϕ about the chosen ground state as:

$$\phi(x) = \frac{1}{\sqrt{2}} \exp\left(\frac{i}{v} \sigma_i \theta^i(x)\right) \begin{pmatrix} 0 \\ v + H(x) \end{pmatrix} \approx \frac{1}{\sqrt{2}} \begin{pmatrix} \theta_1(x) + i\theta_2(x) \\ v + H(x) - i\theta_3(x) \end{pmatrix} \quad (2.42)$$

630 to describe fluctuations from the ground state ϕ_0 . The fields $\theta_i(x)$ represent the
 631 Nambu-Goldstone bosons while $H(x)$ is known as “higgs field.” The fundamental
 632 feature of the parametrization used is that the dependence on the $\theta_i(x)$ fields is
 633 factored out in a global phase that can be eliminated by taking the physical “unitary
 634 gauge” $\theta_i(x) = 0$. Therefore the expansion about the ground state is given by:

$$\phi(x) \frac{1}{\sqrt{2}} \begin{pmatrix} 0 \\ v + H(x) \end{pmatrix} \quad (2.43)$$

635 which when substituted into \mathcal{L}_S (eqn. 2.37) results in a Lagrangian containing the now
 636 massive three gauge bosons W^\pm, Z , one massless gauge boson (photon) and the new
 637 Higgs field (H). The three degrees of freedom corresponding to the Nambu-Goldstone
 638 bosons are now integrated into the massive gauge bosons as their longitudinal polar-
 639 izations which were not available when they were massless particles. The effect by
 640 which vector boson fields acquire mass after an spontaneous symmetry breaking but
 641 without an explicit gauge invariance breaking is known as the “*Higgs mechanism*.”

642 The mechanism was proposed by three independent groups: F.Englert and R.Brout
 643 in August 1964 [36]; P.Higgs in October 1964 [37]; and G.Guralnik, C.Hagen and
 644 T.Kibble in November 1964 [38]; however, its importance was not realized until
 645 S.Glashow [14], A.Salam [15] and S.Weinberg [16] independently proposed that elec-
 646 tromagnetic and weak interactions are two manifestations of a more general interac-
 647 tion called “electroweak interaction” in 1967.

648 2.3.3 Masses of the gauge bosons

649 The mass of the gauge bosons is extracted by evaluating the kinetic part of Lagrangian
 650 \mathcal{L}_S in the ground state (known also as the vacuum expectation value) i.e.

$$\left| \left(\partial_\mu - ig \frac{\sigma_i}{2} W_\mu^i - i \frac{g'}{2} B_\mu \right) \phi_0 \right|^2 = \left(\frac{1}{2} v g \right)^2 W_\mu^+ W^{-\mu} + \frac{1}{8} v^2 (W_\mu^3, B_\mu) \begin{pmatrix} g^2 & -gg' \\ -gg' & g'^2 \end{pmatrix} \begin{pmatrix} W^{3\mu} \\ B^\mu \end{pmatrix} \quad (2.44)$$

651 comparing with the typical mass term for a charged boson $M_W^2 W^+ W^-$

$$M_W = \frac{1}{2} v g. \quad (2.45)$$

The second term in the right side of the eqn.2.44 comprises the masses of the neutral
 bosons, but it needs to be written in terms of the gauge fields Z_μ and A_μ in order to
 be compared to the typical mass terms for neutral bosons, therefore using eqn. 2.29

$$\begin{aligned} \frac{1}{8} v^2 [g^2 (W_\mu^3)^2 - 2gg' W_\mu^3 B^\mu + g'^2 B_\mu^2] &= \frac{1}{8} v^2 [g W_\mu^3 - g' B_\mu]^2 + 0[g' W_\mu^3 + g B_\mu]^2 \quad (2.46) \\ &= \frac{1}{8} v^2 [\sqrt{g^2 + g'^2} Z_\mu]^2 + 0[\sqrt{g^2 + g'^2} A_\mu]^2 \end{aligned}$$

652 and then

$$M_Z = \frac{1}{2}v\sqrt{g^2 + g'^2}, \quad M_A = 0 \quad (2.47)$$

653 2.3.4 Masses of the fermions

654 The lepton mass terms can be generated by introducing a gauge invariant Lagrangian
 655 term describing the Yukawa coupling between the lepton field and the Higgs field:

$$\mathcal{L}_{Yl} = -G_l \left[(\bar{\nu}_l, \bar{l})_L \begin{pmatrix} \phi^+ \\ \phi^0 \end{pmatrix} l_R + \bar{l}_R (\phi^-, \bar{\phi}^0) \begin{pmatrix} \nu_l \\ l \end{pmatrix} \right], \quad l = e, \mu, \tau. \quad (2.48)$$

656 After the SSB and replacing the usual field expansion about the ground state (eqn.2.41)
 657 into \mathcal{L}_{Yl} , the mass term arises

$$\mathcal{L}_{Yl} = -m_l(\bar{l}_L l_R + \bar{l}_R l_L) - \frac{m_l}{v}(\bar{l}_L l_R + \bar{l}_R l_L)H = -m_l \bar{l}l \left(1 + \frac{H}{v}\right) \quad (2.49)$$

658

$$m_l = \frac{G_l}{\sqrt{2}}v \quad (2.50)$$

659 where the additional term represents the lepton-Higgs interaction. The quark masses
 660 are generated in a similar way as lepton masses but for the upper member of the
 661 quark doublet a different Higgs doublet is needed:

$$\phi_c = -i\sigma_2\phi^* = \begin{pmatrix} -\bar{\phi}^0 \\ \phi^- \end{pmatrix}. \quad (2.51)$$

662 Additionally, given that the quark isospin doublets are not constructed in terms of
 663 the mass eigenstates but in terms of the flavor eigenstates as shown in table2.4, the
 664 coupling parameters will be related to the CKM matrix elements; thus the quark
 665 Lagrangian is given by:

$$\mathcal{L}_{Yq} = -G_d^{i,j}(\bar{u}_i, \bar{d}'_i)_L \begin{pmatrix} \phi^+ \\ \phi^0 \end{pmatrix} d_{jR} - G_u^{i,j}(\bar{u}_i, \bar{d}'_i)_L \begin{pmatrix} -\bar{\phi}^0 \\ \phi^- \end{pmatrix} u_{jR} + h.c. \quad (2.52)$$

with $i,j=1,2,3$. After SSB and expansion about the ground state, the diagonal form of \mathcal{L}_{Yq} is:

$$\mathcal{L}_{Yq} = -m_d^i \bar{d}_i d_i \left(1 + \frac{H}{v}\right) - m_u^i \bar{u}_i u_i \left(1 + \frac{H}{v}\right) \quad (2.53)$$

Fermion masses depends on arbitrary couplings G_l and $G_{u,d}$ and are not predicted by the theory.

2.3.5 The Higgs field

After the characterization of the fermions and gauge bosons as well as their interactions, it is necessary to characterize the Higgs field itself. The Lagrangian \mathcal{L}_S in eqn:2.37 written in terms of the gauge bosons is given by

$$\mathcal{L}_S = \frac{1}{4} \lambda v^4 + \mathcal{L}_H + \mathcal{L}_{HV} \quad (2.54)$$

$$\mathcal{L}_H = \frac{1}{2} \partial_\mu H \partial^\mu H - \frac{1}{2} m_H^2 H^2 - \frac{1}{2v} m_H^2 H^3 - \frac{1}{8v^2} m_H^2 H^4 \quad (2.55)$$

$$\mathcal{L}_{HV} = m_H^2 W_\mu^+ W^{\mu-} \left(1 + \frac{2}{v} H + \frac{2}{v^2} H^2\right) + \frac{1}{2} m_Z^2 Z_\mu Z^\mu \left(1 + \frac{2}{v} H + \frac{2}{v^2} H^2\right) \quad (2.56)$$

Property	Value
Electric charge	0
Colour charge	0
Spin	0
Weak isospin	-1/2
Weak hypercharge	1
Parity	1
Mass (GeV/c ²)	125.09 ± 0.21 (stat.) ± 0.11 (syst.)

Table 2.7: Higgs boson properties. Higgs mass is not predicted by the theory and the value here corresponds to the experimental measurement.

677 The mass of the Higgs boson is deduced as usual from the mass term in the Lagrangian
 678 resulting in:

$$m_H = \sqrt{-2\mu^2} = \sqrt{2\lambda}v \quad (2.57)$$

679 however, it too is not predicted by the theory. The experimental efforts to find the
 680 Higgs boson, carried out by the CMS and ATLAS experiments⁸, gave great results
 681 by July of 2012 when the discovery of a new particles was announced and which
 682 is compatible with the Higgs boson predicted by the electroweak theory [39, 40].
 683 Although at the announcement time there were some reservations about calling the
 684 new particle the “Higgs boson”, today this name is widely accepted. The result of
 685 the measurement of the Higgs mass reported by both experiments [41] is in table 2.7.

686 2.3.6 Higgs boson production mechanisms at LHC.

687 This thesis explore the Higgs production at LHC; therefore the overview presented
 688 here will be oriented specifically to the production mechanisms after pp collisions at
 689 LHC.

690 The pp collision at..... to be completed...

691

692 As shown in eqns 2.48, 2.52 and 2.56, the strength of the Higgs-fermion interaction
 693 is proportional to the fermion mass while the strength of the Higgs-gauge boson
 694 interaction is proportional to the square of the gauge boson mass, which implies
 695 that the Higgs production and decay mechanisms are dominated by couplings $H -$
 696 (W, Z, t, b, τ) .

697 In physics, a common approach to study complex systems consist in starting with
 698 a simpler version of them, for which a well known description is available, and add

⁸ CMS stands for Compact Muon Solenoid; ATLAS stand for A Toroidal LHC Apparatus. Both are general experiments held at the Large Hadron Collider(LHC)

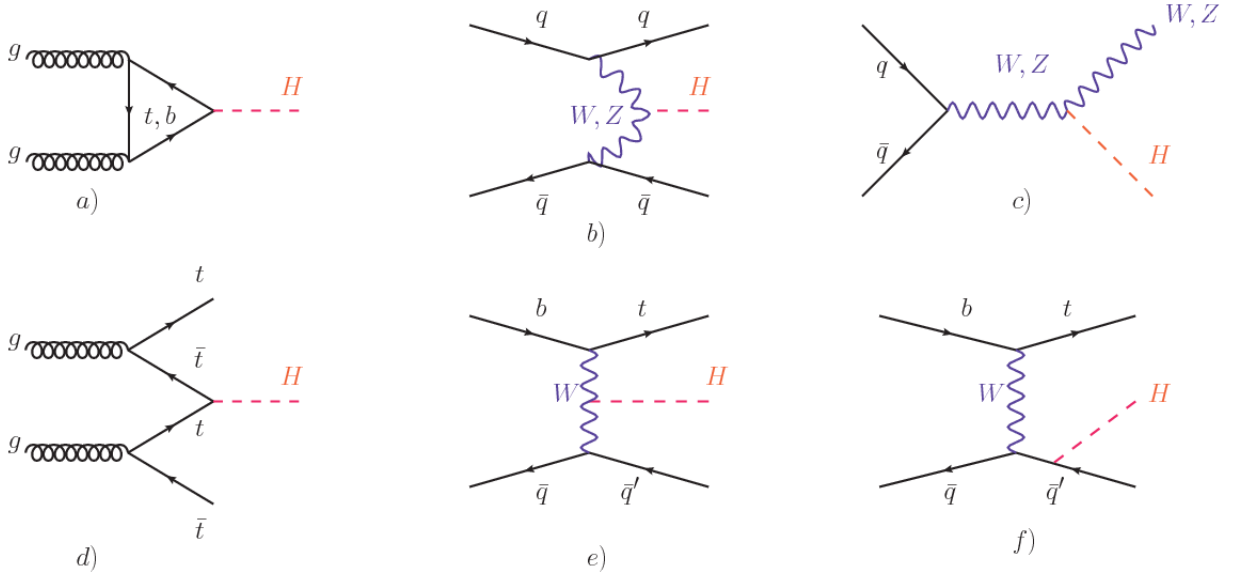


Figure 2.10: Main Higgs production mechanism Feynman diagrams. a) gluon-gluon fusion, b) vector boson fusion (VBF), c) Higgs-strahlung, d) Associated production with a top or bottom quark pair, e-f) associated production with a single top quark.

699 an additional “perturbation” which represent a small deviation from the known be-
 700 havior. If the perturbation is small enough, the physical quantities associated with
 701 the perturbed system are expressed as a series of corrections to those of the simpler
 702 system; therefore, the more terms are considered in the series (the higher order in the
 703 perturbation series), the more precise is the the description of the complex system.
 704 Figure 2.10 shows the Feynman diagrams for the leading order (first order) Higgs
 705 production processes at LHC, while the cross section for Higgs production as a func-
 706 tion of the center of mass-energy (\sqrt{s}) for pp collisions is showed in figure 2.11 left.
 707 The tags NLO (next to leading order), NNLO (next to next to leading order) and
 708 N3LO (next to next to next to leading order) make reference to the order at which
 709 the perturbation series has been considered.
 710 The main production mechanism is the gluon fusion ($pp \rightarrow H$) given that gluons carry
 711 the highest fraction of momentum of the protons in pp colliders. Since the Higgs boson
 712 does not couple to gluons, the mechanism proceeds through the exchange of a virtual

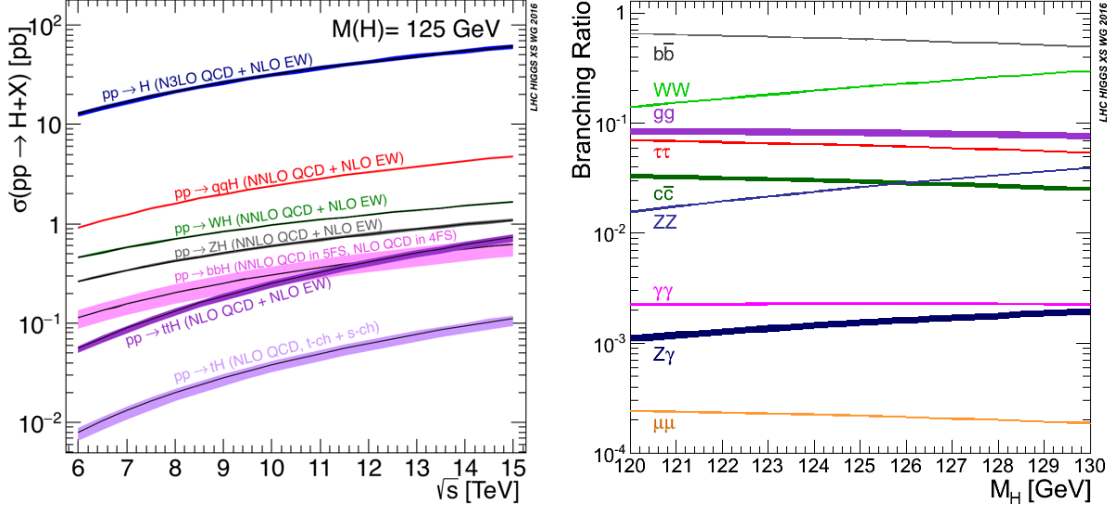


Figure 2.11: Higgs production cross sections (left) and decay branching ratios (right) for the main mechanisms. The VBF is indicated as $q\bar{q}H$ [42].

713 top-quark loop given that for it the coupling is the biggest. Note that in this process,
 714 the Higgs boson is produced alone, which makes this mechanism experimentally clean
 715 when combined with the two-photon or the four-lepton decay channels (see section
 716 2.3.7).

717 Vector boson fusion ($pp \rightarrow q\bar{q}H$) has the second largest production cross section. The
 718 scattering of two fermions is mediated by a weak gauge boson which later emits a Higgs
 719 boson. In the final state, the two fermions tend to be located in a particular region
 720 of the detector which is used as a signature when analyzing the datasets provided by
 721 the experiments. More details about how to identify events of interest in an analysis
 722 will be given in chapter 4.

723 The next production mechanism is Higgs-strahlung ($pp \rightarrow WH, pp \rightarrow ZH$) where two
 724 fermions annihilate to form a weak gauge boson. If the initial fermions have enough
 725 energy, the emergent boson eventually will emit a Higgs boson.

726 The associated production with a top or bottom quark pair and the associated pro-
 727 duction with a single top quark ($pp \rightarrow b\bar{b}H, pp \rightarrow t\bar{t}H, pp \rightarrow tH$) have a smaller cross

728 section than the main three mechanisms above, but they provide a good opportunity
 729 to test the Higgs-top coupling. The analysis reported in this thesis is developed using
 730 these production mechanisms. A detailed description of the tH mechanism will be
 731 given in section 2.4.

732 2.3.7 Higgs decay channels

733 When a particle can decays through several modes, also known as channels, the
 734 probability of decaying through a given channel is quantified by the “branching ratio
 735 (BR)” of the decay channel; thus, the BR is defined as the ratio of number of decays
 736 going through that given channel to the total number of decays. In regard to the
 737 Higgs boson decay, the BR can be predicted with accuracy once the Higgs mass is
 738 known [43, 44]. In figure 2.11 right, a plot of the BR as a function of the Higgs mass
 739 is presented. The largest predicted BR corresponds to the $b\bar{b}$ pair decay channel (see
 740 table 2.8).

Decay channel	Branching ratio	Rel. uncertainty
$H \rightarrow \gamma\gamma$	2.27×10^{-3}	$+5.0\% - 4.9\%$
$H \rightarrow ZZ$	2.62×10^{-2}	$+4.3\% - 4.1\%$
$H \rightarrow W^+W^-$	2.14×10^{-1}	$+4.3\% - 4.2\%$
$H \rightarrow \tau^+\tau^-$	6.27×10^{-2}	$+5.7\% - 5.7\%$
$H \rightarrow b\bar{b}$	5.84×10^{-1}	$+3.2\% - 3.3\%$
$H \rightarrow Z\gamma$	1.53×10^{-3}	$+9.0\% - 8.9\%$
$H \rightarrow \mu^+\mu^-$	2.18×10^{-4}	$+6.0\% - 5.9\%$

Table 2.8: Predicted branching ratios and the relative uncertainty for a SM Higgs boson with $m_H = 125 GeV/c^2$. [21]

⁷⁴² **2.4 Associated Production of Higgs Boson and
⁷⁴³ Single Top Quark.**

⁷⁴⁴ **2.5 The CP-mixing phase**

⁷⁴⁵ Chapter 3

⁷⁴⁶ The CMS experiment at the LHC

⁷⁴⁷ 3.1 Introduction

⁷⁴⁸ Located in the Swiss-French border, the European Council for Nuclear Research
⁷⁴⁹ (CERN) is the largest scientific organization leading the particle physics research.
⁷⁵⁰ About 13000 people in a broad range of fields including users, students, scientists,
⁷⁵¹ engineers among others, contribute to the data taking and analysis, with the goal
⁷⁵² of unveiling the secrets of the nature and revealing the fundamental structure of the
⁷⁵³ universe. CERN is also the home of the Large Hadron Collider (LHC), the largest
⁷⁵⁴ circular particle accelerator around the world, where protons (or heavy ions) traveling
⁷⁵⁵ close to the speed of light, are made to collide. These collisions open a window to
⁷⁵⁶ investigate how particles (and their constituents if they are composite) interact with
⁷⁵⁷ each other, providing clues about the laws of the nature.

⁷⁵⁸ LHC can run in three modes depending on the particles being accelerated

- ⁷⁵⁹ • Proton-Proton collisions (pp) multiple physics experiments .
- ⁷⁶⁰ • Lead-Lead collisions (Pb-Pb) Heavy ion experiments.

761 • Proton-Lead collisions (p-Pb).

762 Figure 3.1 show an overview of the CERN accelerating complex. There are several
 763 accelerating stages before the injection to the LHC ring. In the pp mode, after
 764 removing the electrons from hydrogen atoms in a bottle, protons are accelerated
 765 in the LINAC2 to 50 MeV and then injected into the proton synchrotron booster
 766 (BOOSTER) to reach 1.4 GeV in energy. The next boost is provided at the proton
 767 synchrotron (PS) up to 26 GeV, followed by the injection into the super proton
 768 synchrotron (SPS) where protons are accelerated to 450 GeV. Finally, protons are
 769 injected into the LHC where they are accelerated to the target energy of 6.5 TeV. In
 770 the Pb-Pb mode, the Lead ions are first accelerated in the LINAC3 and then passed as
 771 long pulses to the Low energy ion ring (LEIR) to be converted into short and dense
 772 bunches, each containing 7×10^7 lead ions. LEIR accelerate the bunches from 4.2
 773 MeV to 72 MeV. The ions are then passed to the PS to follow the rest of acceleration
 774 process up to 2.8TeV/n en the LHC ring.

775 3.2 The LHC

776 The LHC is a 27 km ring composed of superconducting magnets and accelerating
 777 structures (among other components) which boost the particles traveling inside it.
 778 It is installed in the same tunnel where the large Electron-Positron (LEP) collider
 779 was located, taking advantage of the existing infraestructure as shown in Figure 3.2.
 780 Two particle beams travel counter-rotating in two separated beam pipes kept at ultra
 781 high vacuum. In 2008, the first set of collisions involved protons with center-of-mass
 782 energy of 7 TeV after which the energy was increased to 8 TeV in 2012 and to 13 TeV
 783 in 2015.

CERN's accelerator complex

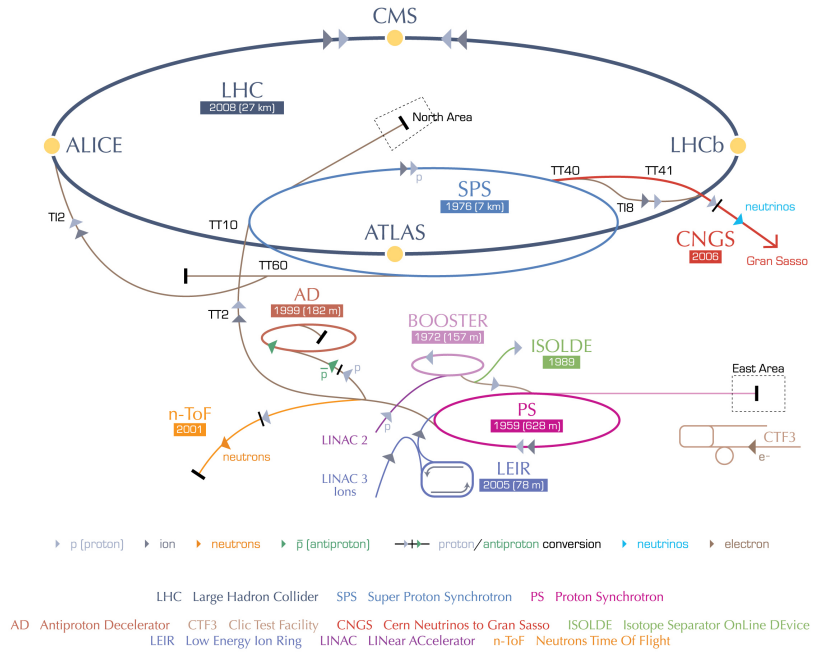
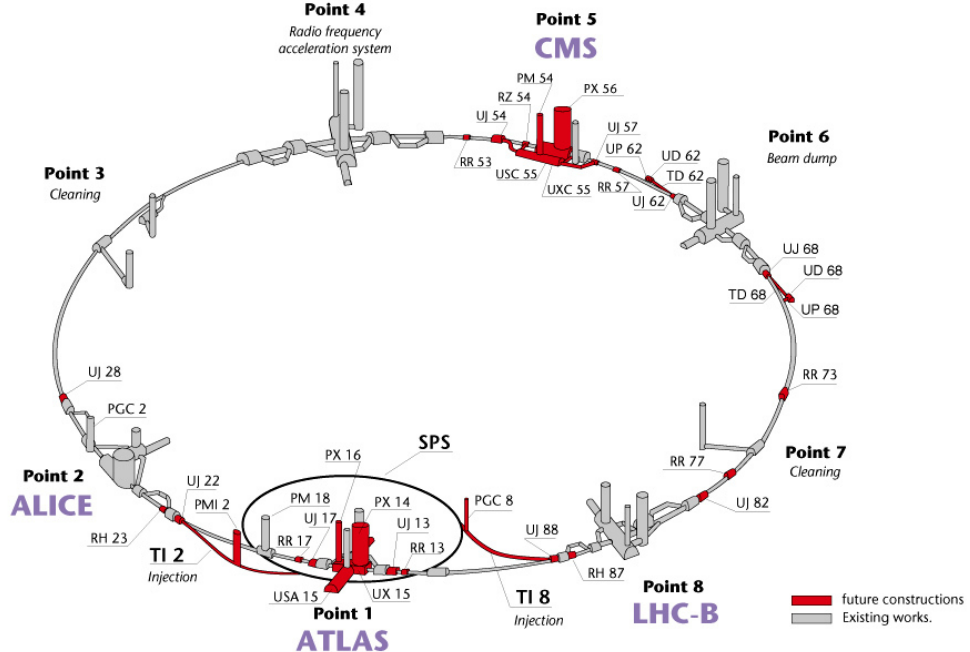


Figure 3.1: ref. C.Lefevre, “The CERN accelerator complex,” (2008). CERN-DI-0812015.

In order to keep the protons in the circular trajectory carrying that amount of energy, strong magnetic fields are needed, bringing the superconductivity into scene. The superconducting dipole magnets used in LHC are made of a NbTi alloy, capable of transporting currents of about 12000 A when cooled at a temperature below 2K by using liquid helium; that current generates a magnetic fields of 8.3 T. Figure 3.3 shows the transverse view of the LHC dipole magnets. Additionally, quadrupole magnets are used to focus the beam and some other magnetic multipoles are used to correct effects generated by the interaction among protons in the beam as well as interactions within the beam pipe.

Regarding to the longitudinal acceleration of the protons, a system of 16 radio-frequency cavities (RF) (8 per beam) is used to accelerate protons. Inside the cavities,

Layout of the LEP tunnel including future LHC infrastructures.



CERN AC _ hf238 _ V02/02/98

Figure 3.2: ref. J.-L. Caron , “Layout of the LEP tunnel including future LHC infrastructures.. L’ensemble du tunnel LEP avec les futures infrastructures LHC.”, <https://cds.cern.ch/record/841542> (Nov, 1993). AC Collection. Legacy of AC. Pictures from 1992 to 2002..

the electromagnetic waves become resonant transferring the maximum energy to the particle flight through it. Cavities are cooled at 4.5 K. On LHC the RF oscillation frequency is 400MHz and the protons are carefully timed so additionally to the acceleration effect the bunch structure of the beam is preserved. The Beam is made of 2808 “bunches” which are packages of 1.15×10^{11} protons ???. If LHC is at full energy, protons with the right energy does not feel any accelerating force but those with a different energy will be accelerated or decelerated to keep them in the bunch. The paths followed by particles during the acceleration process are shown in Figure 3.1.

LHC DIPOLE : STANDARD CROSS-SECTION

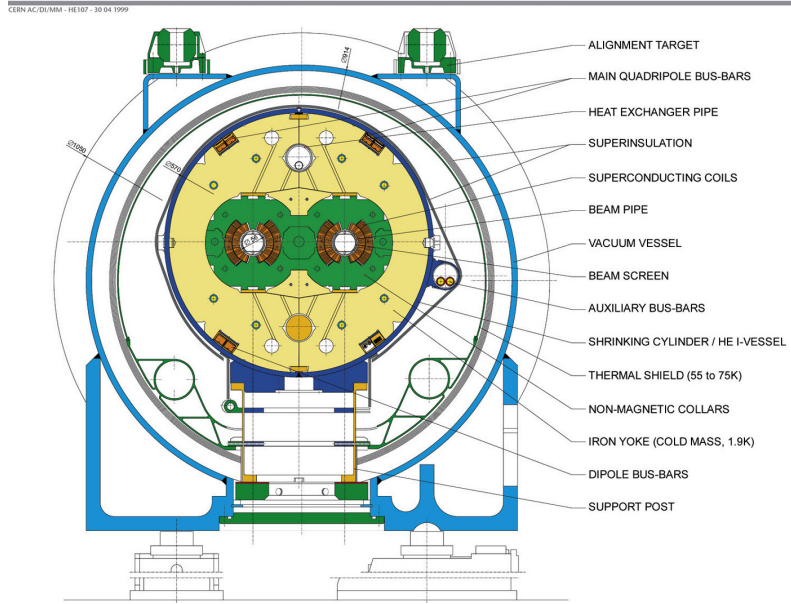


Figure 3.3: ref. ACTeam, “Diagram of an LHC dipole magnet. Schéma d’un aimant dipôle du LHC,” (1999). CERN-DI-9906025.

Once the beams reach the desired energy, they are brought to cross each other producing proton-proton collisions. The bunch crossing happens in precise places where the LHC experiments are located. As seen in Figure 3.2, it was needed to build the caverns for CMS and ATLAS as well as some additional facilities, but most of the initial LEP infrastructure has been used to allocate additional collision points. The highest luminosity is delivered at the CMS (point 5) and ATLAS (point 1) experiments, which are general purpose experiments, enabled to explore physics in any of the collision modes. LHCb (point 8) experiment is optimized to explore B-physics, while ALICE (point 2) is optimized for heavy ion collisions researches; TOTEM (point 5) and LHCf (point 1) are dedicated to forward physics studies and MoEDAL (point 8) is intended for monopoles or massive pseudo stable particles studies.

816 3.3 The CMS experiment

817 The Compact Muon Solenoid (CMS) is a general purpose detector designed to conduct
818 research in a wide range of physics from standard model to new physics like extra
819 dimensions and dark matter. Located at the point 5 in the LHC layout as shown in
820 Figure 3.2, CMS is composed by several detection systems distributed in a cylindrical
821 structure where the main feature is a solenoid magnet made of superconducting cable
822 capable to generate a 3.8 T magnetic field. In total, CMS weight about 14000 tons
823 in a very compact 21.6 m long and 14.6 m diameter cylinder (include areference for
824 CMS TDR). It was built in 15 separated sections at the ground level and lowered
825 to the cavern individually to be assembled. Figure 3.4 show the layout of the CMS
826 detector (CMS TDR).

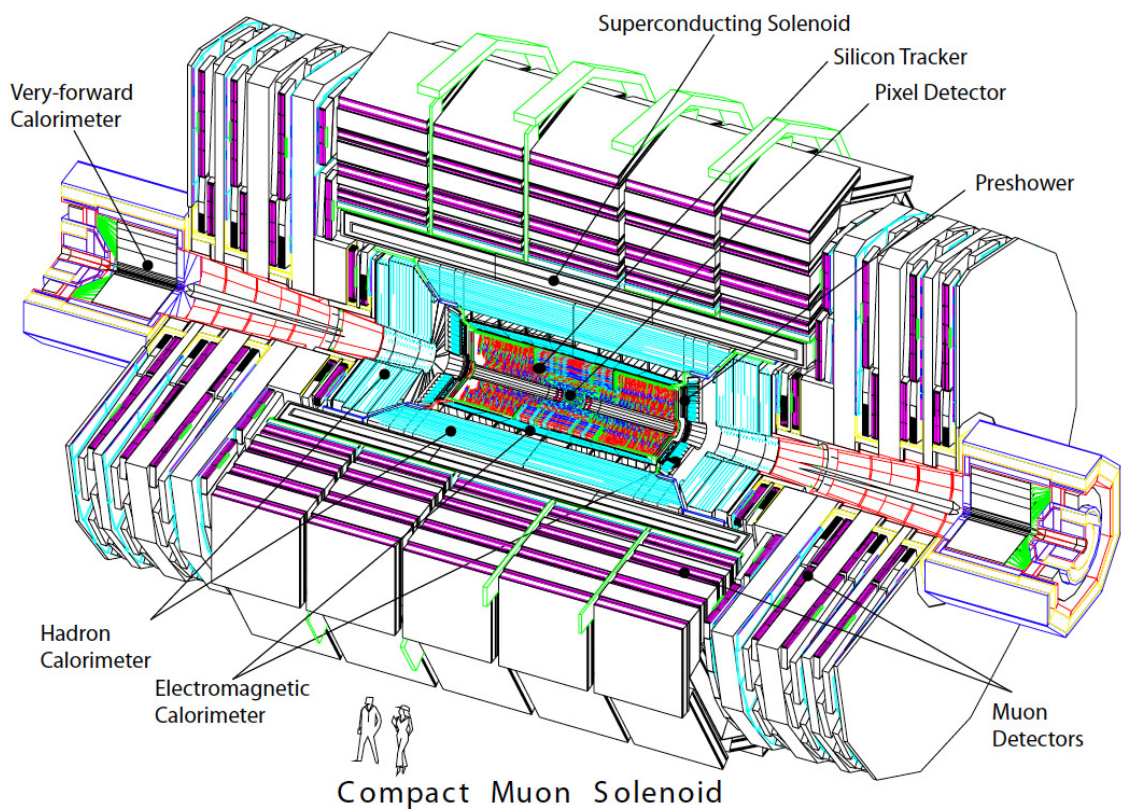


Figure 3.4: ref: CMS Collaboration, “Detector Drawings”, CMS-PHO-GEN-2012-002, <http://cds.cern.ch/record/1433717>, 2012.

827 **Chapter 4**

828 **Search for production of a Higgs
829 boson and a single top quark in
830 multilepton final states in pp
831 collisions at $\sqrt{s} = 13$ TeV**

832 **4.1 Introduction**

833 This chapter present the search for the associated production of a Higgs boson and
834 a single top quark events with three leptons in the final state, targeting Higgs decay
835 modes to WW , ZZ , and $\tau\tau$. The analysis uses the 13 TeV dataset produced in 2016,
836 corresponding to an integrated luminosity of 35.9fb^{-1} . It is based on and expands
837 previous analyses at 8 TeV [45, 46] and searches for associated production of $t\bar{t}$ and
838 Higgs in the same channel [47], and complements searches in other decay channels
839 targeting $H \rightarrow b\bar{b}$ [48].

840 The production cross section of the single top plus Higgs boson (tHq) process

841 is driven by a destructive interference of two main diagrams (see Fig. 4.1), where
 842 the Higgs couples to either the W boson or the top quark. Any deviation from the
 843 standard model (SM) in the Higgs coupling structure could therefore lead to a large
 844 enhancement of the cross section, making this analysis sensitive to such deviations.
 845 A second process, where the Higgs and top quark are accompanied by a W boson
 846 (tHW) has similar behavior, albeit with a weaker interference pattern.

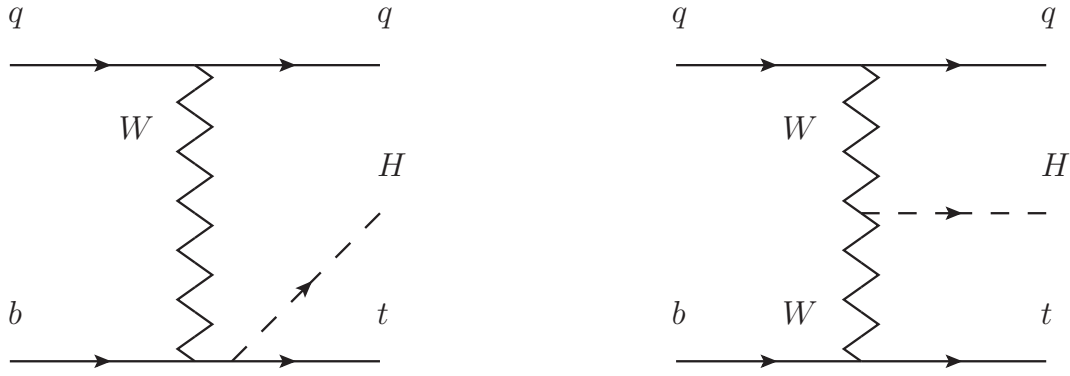


Figure 4.1: The two leading-order diagrams of tHq production.

847 We select events with three leptons and a b tagged jet in the final state. The tHq
 848 signal contribution is then determined in a fit of the observed data to two multivariate
 849 classifier outputs, each trained to discriminate against one of the two dominant back-
 850 grounds of events with non-prompt leptons from $t\bar{t}$ and of associated production of $t\bar{t}$
 851 and vector bosons ($t\bar{t}W$, $t\bar{t}Z$). The fit result is then used to set an upper limit on the
 852 combined $t\bar{t}H$, tHq and tHW production cross section, as a function of the relative
 853 coupling strengths of Higgs and top quark and Higgs and W boson, respectively.

854 4.2 Data and MC Samples

855 The data considered in this analysis were collected by the CMS experiment dur-
 856 ing 2016 and correspond to a total integrated luminosity of 35.9fb^{-1} . Only periods
 857 when the CMS magnet was on were considered when selecting the data samples, that
 858 corresponds to the 23 Sep 2016 (Run B to G) and PromptReco (Run H) versions
 859 of the datasets. The MC samples used in this analysis correspond to the RunI-
 860 ISummer16MiniAODv2 campaign produced with CMSSW 80X. The two signal sam-
 861 ples (for tHq and tHW) were produced with MG5_aMC@NLO (version 5.222), in
 862 leading-order order mode, and are normalized to next-to-leading-order cross sections,
 863 see Tab. 4.1. Each sample is generated with a set of event weights corresponding to
 864 different values of κ_t and κ_V couplings as shown in Tab. 4.2.

865 4.2.1 Full 2016 dataset and MC samples

Sample	σ [pb]	BF
/THQ_Hincl_13TeV-madgraph-pythia8_TuneCUETP8M1/	0.7927	0.324
/THW_Hincl_13TeV-madgraph-pythia8_TuneCUETP8M1/	0.1472	1.0

Table 4.1: Signal samples and their cross section and branching fraction used in this analysis. See Ref. [49] for more details.

866 Different MC generators were used to generate the background processes. The
 867 dominant sources ($t\bar{t}$, $t\bar{t}W$, $t\bar{t}Z$, $t\bar{t}H$) were produced using AMC@NLO interfaced
 868 to PYTHIA8, and are scaled to NLO cross sections. Other processes are simulated
 869 using POWHEG interfaced to PYTHIA, or bare PYTHIA (see table 4.3 and [47]
 870 for more details).

		tHq			tHW		
κ_V	κ_t	sum of weights	cross section [pb]	sum of weights	cross section [pb]	LHE weights	
1.0	-3.0	35.700022	2.991	11.030445	0.6409	LHEweight_wgt[446]	
1.0	-2.0	20.124298	1.706	5.967205	0.3458	LHEweight_wgt[447]	
1.0	-1.5	14.043198	1.205	4.029093	0.2353	LHEweight_wgt[448]	
1.0	-1.25	11.429338	0.9869	3.208415	0.1876	LHEweight_wgt[449]	
1.0	-1.0		0.7927		0.1472		
1.0	-0.75	7.054998	0.6212	1.863811	0.1102	LHEweight_wgt[450]	
1.0	-0.5	5.294518	0.4723	1.339886	0.07979	LHEweight_wgt[451]	
1.0	-0.25	3.818499	0.3505	0.914880	0.05518	LHEweight_wgt[452]	
1.0	0.0	2.627360	0.2482	0.588902	0.03881	LHEweight_wgt[453]	
1.0	0.25	1.719841	0.1694	0.361621	0.02226	LHEweight_wgt[454]	
1.0	0.5	1.097202	0.1133	0.233368	0.01444	LHEweight_wgt[455]	
1.0	0.75	0.759024	0.08059	0.204034	0.01222	LHEweight_wgt[456]	
1.0	1.0	0.705305	0.07096	0.273617	0.01561	LHEweight_wgt[457]	
1.0	1.25	0.936047	0.0839	0.442119	0.02481	LHEweight_wgt[458]	
1.0	1.5	1.451249	0.1199	0.709538	0.03935	LHEweight_wgt[459]	
1.0	2.0	3.335034	0.2602	1.541132	0.08605	LHEweight_wgt[460]	
1.0	3.0	10.516125	0.8210	4.391335	0.2465	LHEweight_wgt[461]	
<hr/>							
1.5	-3.0	45.281492	3.845	13.426212	0.7825	LHEweight_wgt[462]	
1.5	-2.0	27.606715	2.371	7.809713	0.4574	LHEweight_wgt[463]	
1.5	-1.5	20.476088	1.784	5.594971	0.3290	LHEweight_wgt[464]	
1.5	-1.25	17.337465	1.518	4.635978	0.2749	LHEweight_wgt[465]	
1.5	-1.0	14.483302	1.287	3.775902	0.2244	LHEweight_wgt[466]	
1.5	-0.75	11.913599	1.067	3.014744	0.1799	LHEweight_wgt[467]	
1.5	-0.5	9.628357	0.874	2.352505	0.1410	LHEweight_wgt[468]	
1.5	-0.25	7.627574	0.702	1.789184	0.1081	LHEweight_wgt[469]	
1.5	0.0	5.911882	0.5577	1.324946	0.08056	LHEweight_wgt[470]	
1.5	0.25	4.479390	0.4365	0.959295	0.05893	LHEweight_wgt[471]	
1.5	0.5	3.331988	0.3343	0.692727	0.04277	LHEweight_wgt[472]	
1.5	0.75	2.469046	0.2558	0.525078	0.03263	LHEweight_wgt[473]	
1.5	1.0	1.890565	0.2003	0.456347	0.02768	LHEweight_wgt[474]	
1.5	1.25	1.596544	0.1689	0.486534	0.02864	LHEweight_wgt[475]	
1.5	1.5	1.586983	0.1594	0.615638	0.03509	LHEweight_wgt[476]	
1.5	2.0	2.421241	0.2105	1.170602	0.06515	LHEweight_wgt[477]	
1.5	3.0	7.503280	0.5889	3.467546	0.1930	LHEweight_wgt[478]	
<hr/>							
0.5	-3.0	27.432685	2.260	8.929074	0.5136	LHEweight_wgt[479]	
0.5	-2.0	13.956013	1.160	4.419093	0.2547	LHEweight_wgt[480]	
0.5	-1.5	8.924438	0.7478	2.757611	0.1591	LHEweight_wgt[481]	
0.5	-1.25	6.835341	0.5726	2.075247	0.1204	LHEweight_wgt[482]	
0.5	-1.0	5.030704	0.4273	1.491801	0.08696	LHEweight_wgt[483]	
0.5	-0.75	3.510528	0.2999	1.007273	0.05885	LHEweight_wgt[484]	
0.5	-0.5	2.274811	0.1982	0.621663	0.03658	LHEweight_wgt[485]	
0.5	-0.25	1.323555	0.1189	0.334972	0.01996	LHEweight_wgt[486]	
0.5	0.0	0.656969	0.06223	0.147253	0.008986	LHEweight_wgt[487]	
0.5	0.25	0.274423	0.02830	0.058342	0.003608	LHEweight_wgt[488]	
0.5	0.5	0.176548	0.01778	0.068404	0.003902	LHEweight_wgt[489]	
0.5	0.75	0.363132	0.03008	0.177385	0.009854	LHEweight_wgt[490]	
0.5	1.0	0.834177	0.06550	0.385283	0.02145	LHEweight_wgt[491]	
0.5	1.25	1.589682	0.1241	0.692099	0.03848	LHEweight_wgt[492]	
0.5	1.5	2.629647	0.2047	1.097834	0.06136	LHEweight_wgt[493]	
0.5	2.0	5.562958	0.4358	2.206057	0.1246	LHEweight_wgt[494]	
0.5	3.0	14.843102	1.177	5.609519	0.3172	LHEweight_wgt[495]	

Table 4.2: κ_V and κ_t combinations generated for the two signal samples and their NLO cross sections. The tHq cross section is multiplied by the branching fraction of the enforced leptonic decay of the top quark (0.324). See also Ref. [49].

Sample	σ [pb]
TTWJetsToLNu_TuneCUETP8M1_13TeV-amcatnloFXFX-madspin-pythia8	0.2043
TTZToLLNuNu_M-10_TuneCUETP8M1_13TeV-amcatnlo-pythia8	0.2529
ttHJetToNonbb_M125_13TeV_amcatnloFXFX_madspin_pythia8_mWCutfix /store/cmst3/group/susy/gpetrucc/13TeV/u/TTLL_m1to10_LO_NoMS_for76X/	0.2151 0.0283
WGToLNuG_TuneCUETP8M1_13TeV-madgraphMLM-pythia8	585.8
ZGTo2LG_TuneCUETP8M1_13TeV-amcatnloFXFX-pythia8	131.3
TGJets_TuneCUETP8M1_13TeV_amcatnlo_madspin_pythia8	2.967
TGJets_TuneCUETP8M1_13TeV_amcatnlo_madspin_pythia8	2.967
TTGJets_TuneCUETP8M1_13TeV-amcatnloFXFX-madspin-pythia8	3.697
WpWpJJ_EWK-QCD_TuneCUETP8M1_13TeV-madgraph-pythia8	0.03711
ZZZ_TuneCUETP8M1_13TeV-amcatnlo-pythia8	0.01398
WWZ_TuneCUETP8M1_13TeV-amcatnlo-pythia8	0.1651
WZZ_TuneCUETP8M1_13TeV-amcatnlo-pythia8	0.05565
WW_DoubleScattering_13TeV-pythia8	1.64
tZq_ll_4f_13TeV-amcatnlo-pythia8_TuneCUETP8M1	0.0758
ST_tWll_5f_LO_13TeV-MadGraph-pythia8	0.01123
TTTT_TuneCUETP8M1_13TeV-amcatnlo-pythia8	0.009103
WZTo3LNu_TuneCUETP8M1_13TeV-powheg-pythia8	4.4296
ZZTo4L_13TeV_powheg_pythia8	1.256
TTJets_SingleLeptFromTbar_TuneCUETP8M1_13TeV-madgraphMLM-pythia8	182.1754
TTJets_SingleLeptFromT_TuneCUETP8M1_13TeV-madgraphMLM-pythia8	182.1754
TTJets_DiLept_TuneCUETP8M1_13TeV-madgraphMLM-pythia8	87.3
DYJetsToLL_M-10to50_TuneCUETP8M1_13TeV-amcatnloFXFX-pythia8	18610
DYJetsToLL_M-50_TuneCUETP8M1_13TeV-madgraphMLM-pythia8	6024
WJetsToLNu_TuneCUETP8M1_13TeV-amcatnloFXFX-pythia8	61526.7
ST_tW_top_5f_inclusiveDecays_13TeV-powheg-pythia8_TuneCUETP8M1	35.6
ST_tW_antitop_5f_inclusiveDecays_13TeV-powheg-pythia8_TuneCUETP8M1	35.6
ST_t-channel_4f_leptonDecays_13TeV-amcatnlo-pythia8_TuneCUETP8M1	70.3144
ST_t-channel_antitop_4f_leptonDecays_13TeV-powheg-pythia8_TuneCUETP8M1	26.2278
ST_s-channel_4f_leptonDecays_13TeV-amcatnlo-pythia8_TuneCUETP8M1	3.68064
WWTo2L2Nu_13TeV-powheg	10.481

Table 4.3: List of background samples used in this analysis (CMSSW 80X). In the first section of the table are listed the samples of the processes for which we use the simulation to extract the final yields and shapes, in the second section the samples of the processes we will estimate from data. The MC simulation is used to design the data driven methods and derive the associated systematics.

Sample	σ [pb]
ttWJets_13TeV_madgraphMLM	0.6105
ttZJets_13TeV_madgraphMLM	0.5297/0.692

Table 4.4: Leading-order $t\bar{t}W$ and $t\bar{t}Z$ samples used in the signal BDT training.

Three lepton and Four lepton
HLT_DiMu9_Ele9_CaloIdL_TrackIdL_v*
HLT_Mu8_DiEle12_CaloIdL_TrackIdL_v*
HLT_TripleMu_12_10_5_v*
HLT_Ele16_Ele12_Ele8_CaloIdL_TrackIdL_v*
HLT_Mu23_TrkIsoVVL_Ele8_CaloIdL_TrackIdL_IsoVL_v*
HLT_Mu23_TrkIsoVVL_Ele8_CaloIdL_TrackIdL_IsoVL_DZ_v*
HLT_Mu8_TrkIsoVVL_Ele23_CaloIdL_TrackIdL_IsoVL_v*
HLT_Mu8_TrkIsoVVL_Ele23_CaloIdL_TrackIdL_IsoVL_DZ_v*
HLT_Ele23_Ele12_CaloIdL_TrackIdL_IsoVL_DZ_v*
HLT_Mu17_TrkIsoVVL_Mu8_TrkIsoVVL_DZ_v*
HLT_Mu17_TrkIsoVVL_TkMu8_TrkIsoVVL_DZ_v*
HLT_IsoMu22_v*
HLT_IsoTkMu22_v*
HLT_IsoMu22_eta2p1_v*
HLT_IsoTkMu22_eta2p1_v*
HLT_IsoMu24_v*
HLT_IsoTkMu24_v*
HLT_Ele27_WPTight_Gsf_v*
HLT_Ele25_eta2p1_WPTight_Gsf_v*
HLT_Ele27_eta2p1_WPLoose_Gsf_v*

Table 4.5: Table of high-level triggers that we consider in the analysis.

4.2.2 Triggers

We consider online-reconstructed events triggered by one, two, or three leptons. Single-lepton triggers are included to boost the acceptance of events where the p_T of the sub-leading lepton falls below the threshold of the double-lepton triggers. Additionally, by including double-lepton triggers in the ≥ 3 lepton category, as well as single-lepton triggers in all categories, we increase the efficiency, considering the logical “or” of the trigger decisions of all the individual triggers in a given category. Tab. 4.5 shows the lowest-threshold non-prescaled triggers present in the High-Level Trigger (HLT) menus for both Monte-Carlo and data in 2016.

4.2.2.1 Trigger efficiency scale factors

The efficiency of events to pass the trigger is measured in simulation (trivially using generator information) and in the data (using event collected by an uncorrelated

Category	Scale Factor
ee	1.01 ± 0.02
e μ	1.01 ± 0.01
$\mu\mu$	1.00 ± 0.01
3l	1.00 ± 0.03

Table 4.6: Trigger efficiency scale factors and associated uncertainties, shown here rounded to the nearest percent.

883 MET trigger). Small differences between the data and MC efficiencies are corrected
 884 by applying scale factors as shown in Tab. 4.6. The exact procedure and control plots
 885 are documented in [50] for the current analysis.

886 4.3 Object Identification and event selection

887 4.3.1 Jets and b tagging

888 The analysis uses anti- k_t (0.4) particle-flow (PF) jets, corrected for charged hadrons
 889 not coming from the primary vertex (charged hadron subtraction), and having jet
 890 energy corrections (`Summer16_23Sep2016V3`) applied as a function of the jet E_T and
 891 η . Jets are only considered if they have a transverse energy above 25GeV.

892 In addition, they are required to be separated from any lepton candidates passing
 893 the fakeable object selections (see Tables 4.7 and 4.8) by $\Delta R > 0.4$.

894 The loose and medium working points of the CSV b-tagging algorithm are used to
 895 identify b jets. Data/simulation differences in the b tagging performance are corrected
 896 by applying per-jet weights to the simulation, dependent on the jet p_T , eta, b tagging
 897 discriminator, and flavor (from simulation truth) [51]. The per-event weight is taken
 898 as the product of the per-jet weights, including those of the jets associated to the
 899 leptons. More details can be found in the corresponding $t\bar{t}H$ documentation [47, 50].

900 **4.3.2 Lepton selection**

Cut	Loose	Fakeable object	Tight
$ \eta < 2.4$	✓	✓	✓
p_T	$> 5\text{GeV}$	$> 15\text{GeV}$	$> 15\text{GeV}$
$ d_{xy} < 0.05 \text{ (cm)}$	✓	✓	✓
$ d_z < 0.1 \text{ (cm)}$	✓	✓	✓
$\text{SIP}_{3D} < 8$	✓	✓	✓
$I_{\text{mini}} < 0.4$	✓	✓	✓
is Loose Muon	✓	✓	✓
jet CSV	—	< 0.8484	< 0.8484
is Medium Muon	—	—	✓
tight-charge	—	—	✓
lepMVA > 0.90	—	—	✓

Table 4.7: Requirements on each of the three muon selections. In the cases where the cut values change between the selections, those values are listed in the table. Otherwise, whether the cut is applied is indicated. For the two p_T^{ratio} and CSV rows, the cuts marked with a † are applied to leptons that fail the lepton MVA cut, while the loose cut value is applied to those that pass the lepton MVA cut.

901 The lepton reconstruction and selection is identical to that used in the $t\bar{t}H$ mul-
 902 tilepton analysis, as documented in Refs. [47, 50]. For details on the reconstruction
 903 algorithms, isolation, pileup mitigation, and a description of the lepton MVA discrim-
 904 inator and validation plots thereof, we refer to that document since they are out of
 905 the scope of this thesis. Three different selections are defined both for the electron
 906 and muon object identification: the *Loose*, *Fakeable Object*, and *Tight* selection. As
 907 described in more detail later, these are used for event level vetoes, the fake rate
 908 estimation application region, and the final signal selection, respectively. The p_T of
 909 fakeable objects is defined as $0.85 \times p_T(\text{jet})$, where the jet is the one associated to the
 910 lepton object. This mitigates the dependence of the fake rate on the momentum of
 911 the fakeable object and thereby improves the precision of the method.

912 Tables 4.7 and 4.8 list the full criteria for the different selections of muons and
 913 electrons.

Cut	Loose	Fakeable Object	Tight
$ \eta < 2.5$	✓	✓	✓
p_T	$> 7\text{GeV}$	$> 15\text{GeV}$	$> 15\text{GeV}$
$ d_{xy} < 0.05 \text{ (cm)}$	✓	✓	✓
$ d_z < 0.1 \text{ (cm)}$	✓	✓	✓
$\text{SIP}_{3D} < 8$	✓	✓	✓
$I_{\text{mini}} < 0.4$	✓	✓	✓
MVA ID $> (0.0, 0.0, 0.7)$	✓	✓	✓
$\sigma_{i\eta i\eta} < (0.011, 0.011, 0.030)$	—	✓	✓
$\text{H/E} < (0.10, 0.10, 0.07)$	—	✓	✓
$\Delta\eta_{in} < (0.01, 0.01, 0.008)$	—	✓	✓
$\Delta\phi_{in} < (0.04, 0.04, 0.07)$	—	✓	✓
$-0.05 < 1/E - 1/p < (0.010, 0.010, 0.005)$	—	✓	✓
p_T^{ratio}	—	$> 0.5 \dagger / -$	—
jet CSV	—	$< 0.3 \dagger / < 0.8484$	< 0.8484
tight-charge	—	—	✓
conversion rejection	—	—	✓
Number of missing hits	< 2	$== 0$	$== 0$
lepMVA > 0.90	—	—	✓

Table 4.8: Criteria for each of the three electron selections. In cases where the cut values change between selections, those values are listed in the table. Otherwise, whether the cut is applied is indicated. In some cases, the cut values change for different η ranges. These ranges are $0 < |\eta| < 0.8$, $0.8 < |\eta| < 1.479$, and $1.479 < |\eta| < 2.5$ and the respective cut values are given in the form (value₁, value₂, value₃).

914 4.3.3 Lepton selection efficiency

915 Efficiencies of reconstruction and selecting loose leptons are measured both for muons
 916 and electrons using a tag and probe method on both data and MC, using $Z \rightarrow \ell^+\ell^-$.
 917 Corresponding scale factors are derived from the ratio of efficiencies and applied to the
 918 selected These. Events are produced for the leptonic SUSY analyses using equivalent
 919 lepton selections and recycled for the $t\bar{t}H$ analysis as well as for this analysis. The
 920 efficiencies of applying the tight selection as defined in Tables 4.7 and 4.8, on the
 921 loose leptons are determined again by using a tag and probe method on a sample of
 922 DY-enriched events. They are documented for the $t\bar{t}H$ analysis in Ref. [50] and are
 923 exactly equivalent for this analysis.

924 4.4 Background predictions

925 The modeling of reducible and irreducible backgrounds in this analysis uses the exact
 926 methods, analysis code, and ROOT trees used for the $t\bar{t}H$ multilepton analysis. We
 927 give a brief description of the methods and refer to the documentation of that analysis
 928 in Refs. [47, 50] for any details.

929 The backgrounds in three-lepton final states can be split in two broad categories:
 930 irreducible backgrounds with genuine prompt leptons (i.e. from on-shell W and Z
 931 boson decays); and reducible backgrounds where at least one of the leptons is “non-
 932 prompt”, i.e. produced within a hadronic jet, either a genuine lepton from heavy
 933 flavor decays, or simply mis-reconstructed jets.

934 Irreducible backgrounds can be reliably estimated directly from Monte-Carlo sim-
 935 ulated events, using higher-order cross sections or data control regions for the overall
 936 normalization. This is done in this analysis for all backgrounds involving prompt lep-
 937 tons: $t\bar{t}W$, $t\bar{t}Z$, $t\bar{t}H$, WZ , ZZ , $W^\pm W^\pm qq$, $t\bar{t}t\bar{t}$, tZq , tZW , WWW , WWZ , WZZ ,
 938 ZZZ .

939 Reducible backgrounds, on the other hand, are not well predicted by simulation,
 940 and are estimated using data-driven methods. In the case of non-prompt leptons, a
 941 fake rate method is used, where the contribution to the final selection is estimated by
 942 extrapolating from a sideband (or “application region”) with a looser lepton definition
 943 (the fakeable object definitions in Tabs. 4.7 and 4.8) to the signal selection. The tight-
 944 to-loose ratios (or “fake rates”) are measured in several background dominated data
 945 events with dedicated triggers, subtracting the residual prompt lepton contribution
 946 using MC. Non-prompt leptons in our signal regions are predominantly produced in $t\bar{t}$
 947 events, with a much smaller contribution, from Drell–Yan production. The systematic
 948 uncertainty on the normalization of the non-prompt background estimation is on the

order of 50%, and thereby one of the dominant limitations on the performance of multilepton analyses in general and this analysis in particular. It consists of several individual sources, such as the result of closure tests of the method using simulated events, limited statistics in the data control regions due to necessary prescaling of lepton triggers, and the uncertainty in the subtraction of residual prompt leptons from the control region.

The fake background where the leptons pass the looser selection are weighted according to how many of them fail the tight criteria. Events with a single failing lepton are weighted with the factor $f/(1-f)$ for the estimate to the tight selection region, where f is the fake rate. Events with two failing leptons are given the negative weight $-f_i f_j / (1-f_i)(1-f_j)$, and for three leptons the weight is positive and equal to the product of $f/(1-f)$ factor evaluated for each failing lepton.

Figures 4.2 show the distributions of some relevant kinematic variables, normalized to the cross section of the respective processes and to the integrated luminosity.

4.5 Signal discrimination

The tHq signal is separated from the main backgrounds using a boosted decision tree (BDT) classifier, trained on simulated signal and background events. A set of discriminating variables are given as input to the BDT which produces a output distribution maximizing the discrimination power. Table 4.9 lists the input variables used while Figures 4.3 show their distributions for the relevant signal and background samples, for the three lepton channel. Two BDT classifiers are trained for the two main backgrounds expected in the analysis: events with prompt leptons from $t\bar{t}W$ and $t\bar{t}Z$ (also referred to as $t\bar{t}V$), and events with non-prompt leptons from $t\bar{t}$. The datasets used in the training are the tHq signal (see Tab. 4.1), and LO MADGRAPH samples

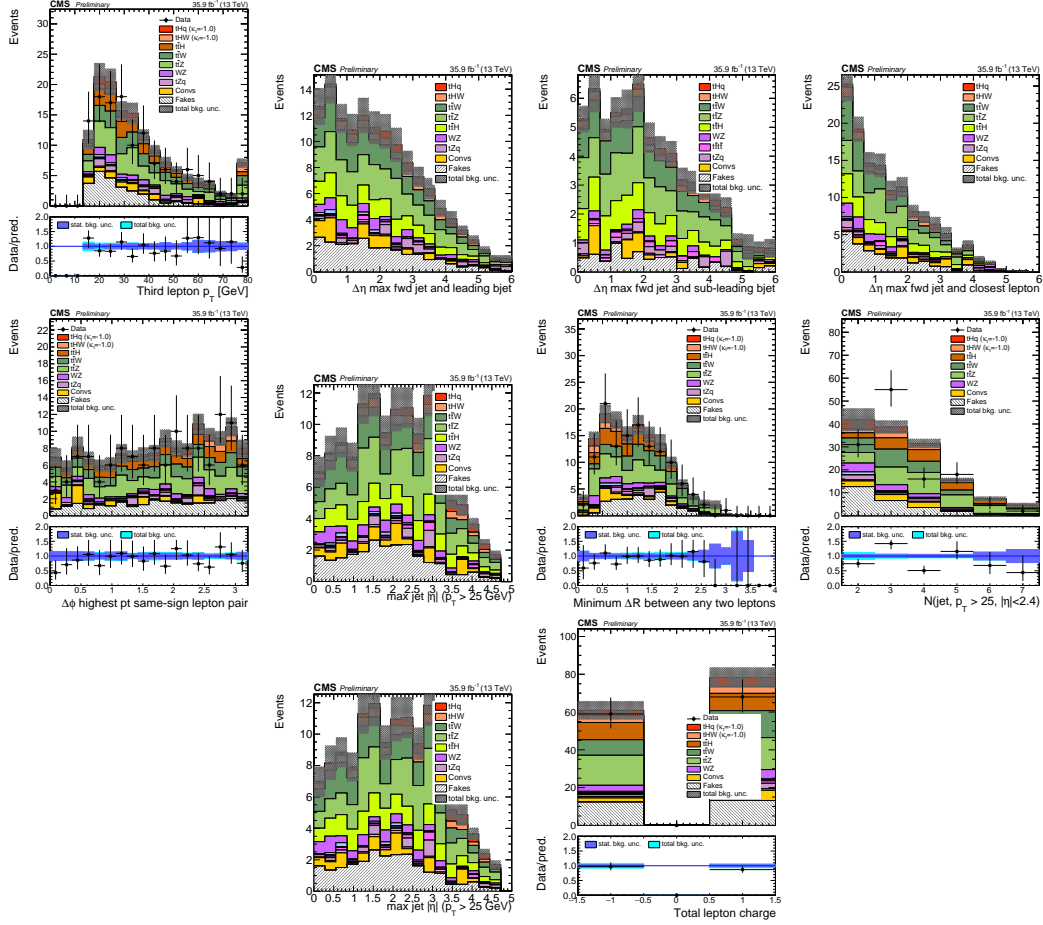


Figure 4.2: Distributions of input variables to the BDT for signal discrimination, three lepton channel, normalized to their cross section and to 35.9 fb^{-1} .

of $t\bar{t}W$ and $t\bar{t}Z$, in an admixture proportional to their respective cross sections (see Tab. 4.4).

The MVA analysis consist of two stages: first a “training” where the MVA method is trained to discriminate between simulated signal and background events, then a “test” stage where the trained algorithm is used to classify different events from the samples. The sample is obtained from a pre-selection (see Tab. ?? with pre-selection cuts). Figures 4.4 show the input variables distributions as seen by the MVA algorithm. Note that in contrast to the distributions in Fig. 4.3 only the main backgrounds ($t\bar{t}$ from simulation, $t\bar{t}V$) are included.

Variable name	Description
nJet25	Number of jets with $p_T > 25$ GeV, $ \eta < 2.4$
MaxEtaJet25	Maximum $ \eta $ of any (non-CSV-loose) jet with $p_T > 25$ GeV
totCharge	Sum of lepton charges
nJetEta1	Number of jets with $ \eta > 1.0$, non-CSV-loose
detaFwdJetBJet	$\Delta\eta$ between forward light jet and hardest CSV loose jet
detaFwdJet2BJet	$\Delta\eta$ between forward light jet and second hardest CSV loose jet (defaults to -1 in events with only one CSV loose jet)
detaFwdJetClosestLep	$\Delta\eta$ between forward light jet and closest lepton
dphiHighestPtSSPair	$\Delta\phi$ of highest p_T same-sign lepton pair
minDRll	minimum ΔR between any two leptons
Lep3Pt/Lep2Pt	p_T of the 3 rd lepton (2 nd for ss2l)

Table 4.9: MVA input discriminating variables

982 Note that splitting the training in two groups reveals that some variables show
 983 opposite behavior for the two background sources; potentially screening the discrimi-
 984 nation power if they were to be used in a single discriminant. For some other variables
 985 the distributions are similar in both background cases.

986 From table 4.9, it is clear that the input variables are correlated to some extend.
 987 These correlations play an important role for some MVA methods like the Fisher
 988 discriminant method in which the first step consist of performing a linear transfor-
 989 mation to an phase space where the correlations between variables are removed. In
 990 case a boosted decision tree (BDT) method however, correlations do not affect the
 991 performance. Figure 4.6 show the linear correlation coefficients for signal and back-
 992 ground for the two training cases (the signal values are identical by construction). As
 993 expected, strong correlations appears for variables related to the forward jet activity.
 994 Same trend is seen in case of the same sign dilepton channel in Figure ??.

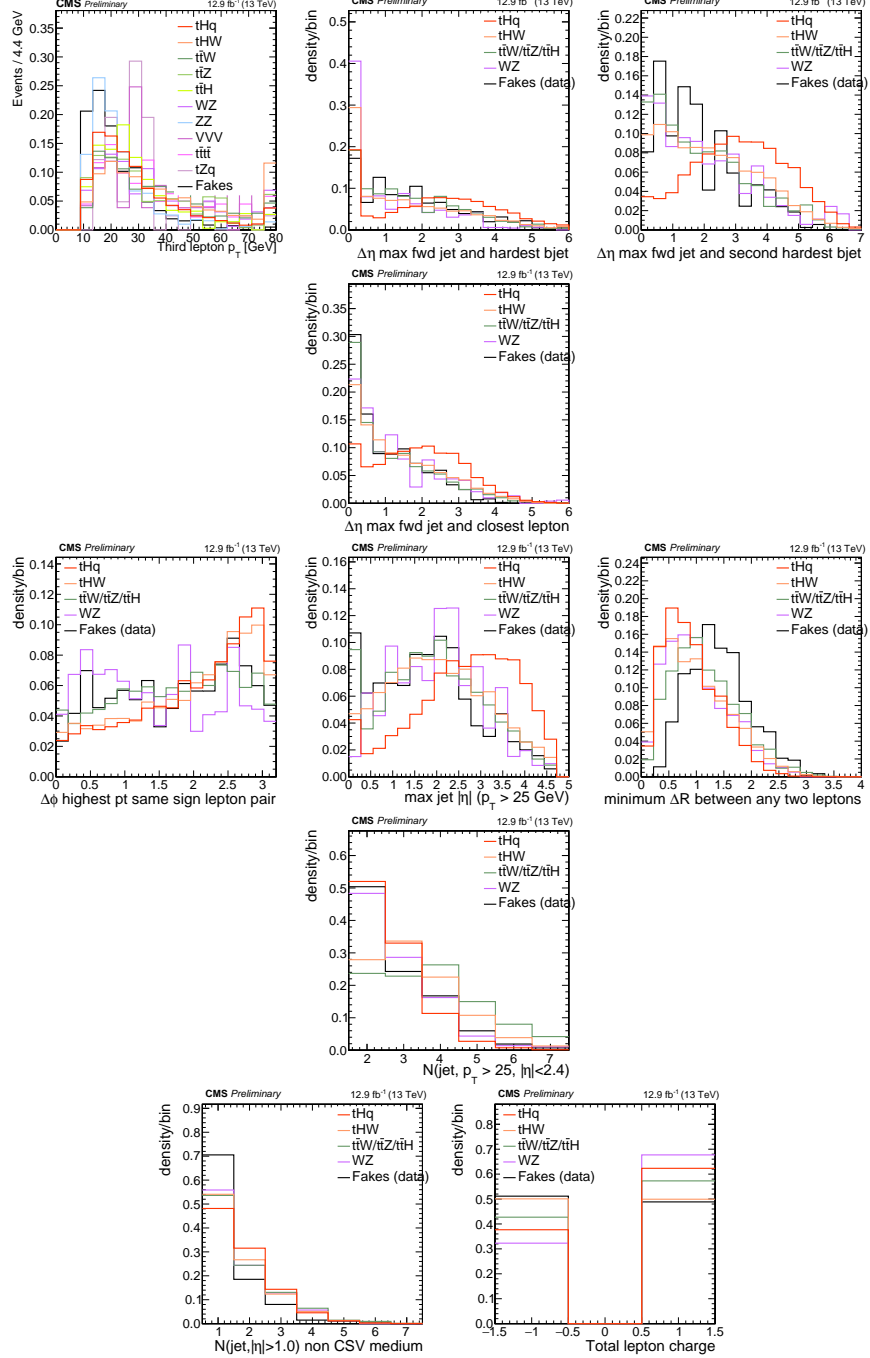


Figure 4.3: Distributions of input variables to the BDT for signal discrimination, three lepton channel.

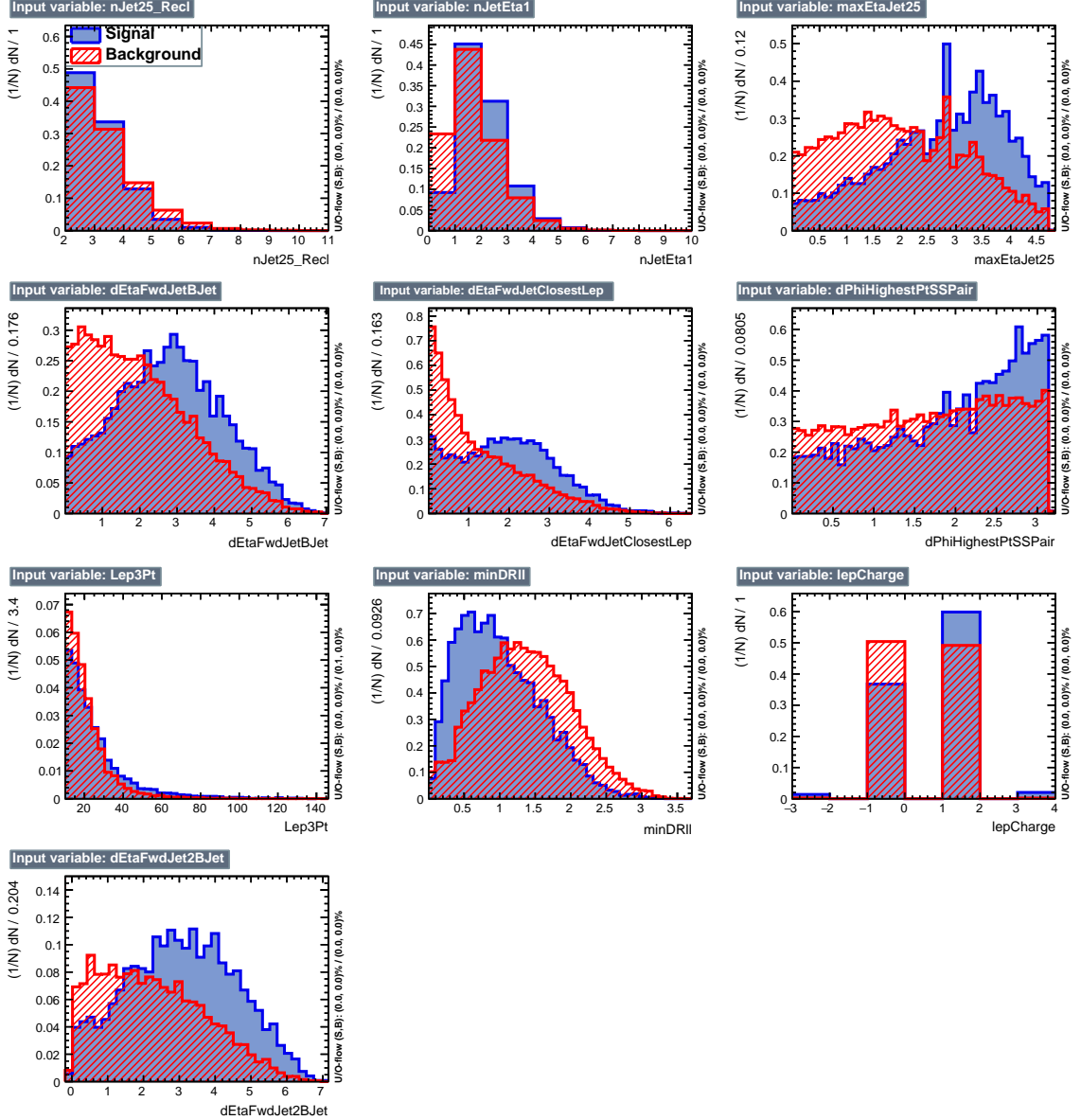


Figure 4.4: BDT inputs as seen by TMVA (signal, in blue, is tHq , background, in red, is $t\bar{t}$) for the three lepton channel, discriminated against $t\bar{t}$ (fakes) background.

995 4.5.1 Classifiers response

996 Several MVA algorithms were evaluated to determine the most appropriate method
 997 for this analysis. The plots in Fig. 4.7 (top) show the background rejection as a
 998 function of the signal efficiency for $t\bar{t}$ and $t\bar{t}V$ trainings (ROC curves) for the different

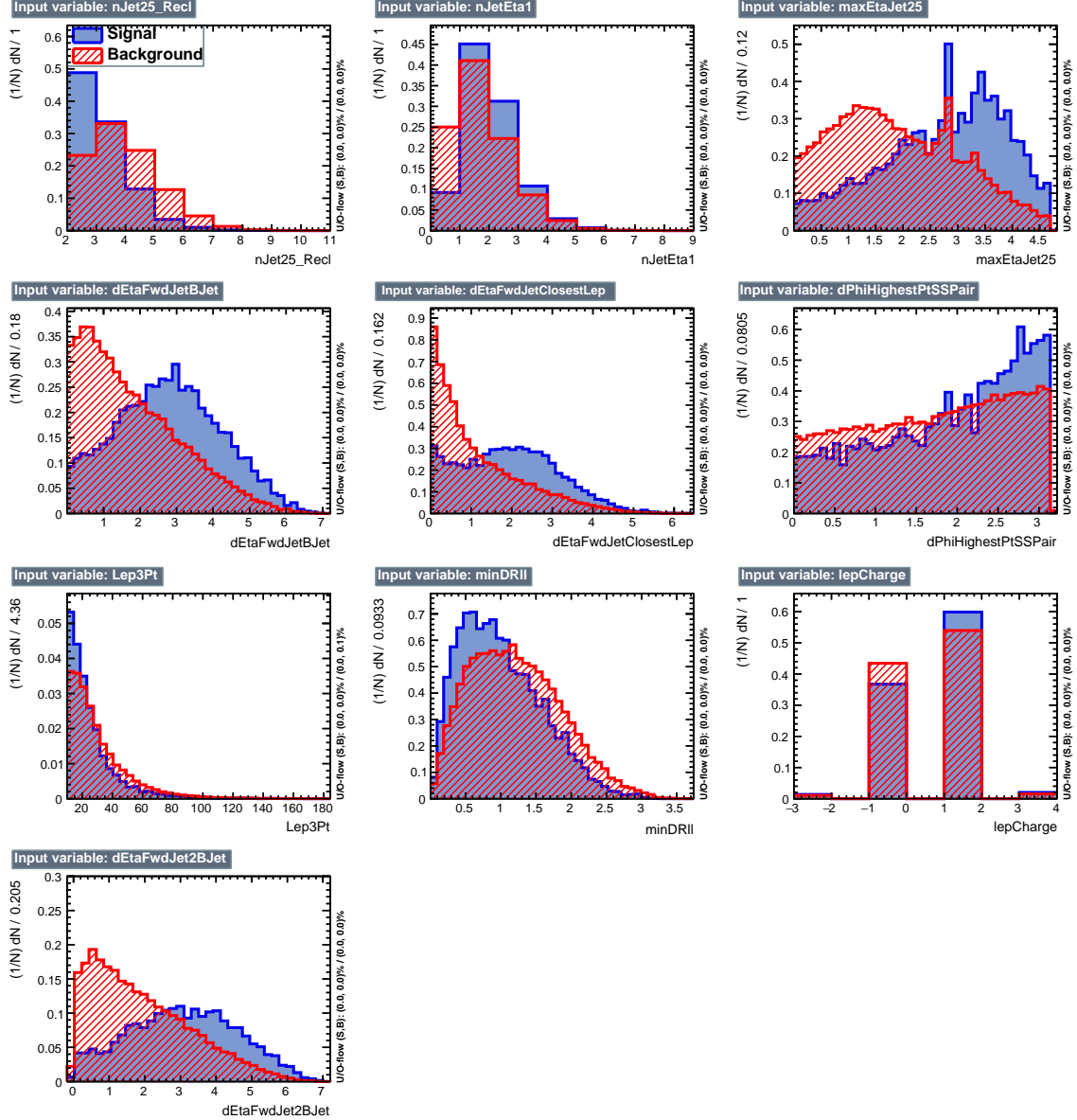


Figure 4.5: BDT inputs as seen by TMVA (signal, in blue, is tHq , background, in red, is $t\bar{t}W+t\bar{t}Z$) for the three lepton channel, discriminated against $t\bar{t}V$ background.

999 algorithms that were evaluated.

1000 In both cases the gradient boosted decision tree (“BDTA_GRAD”) classifier offers
 1001 the best results, followed by an adaptive BDT classifier (“BDTA”). The BDTA_GRAD
 1002 classifier output distributions for signal and backgrounds are shown on the bottom of
 1003 Fig. 4.7. As expected, a good discrimination power is obtained using default discrim-

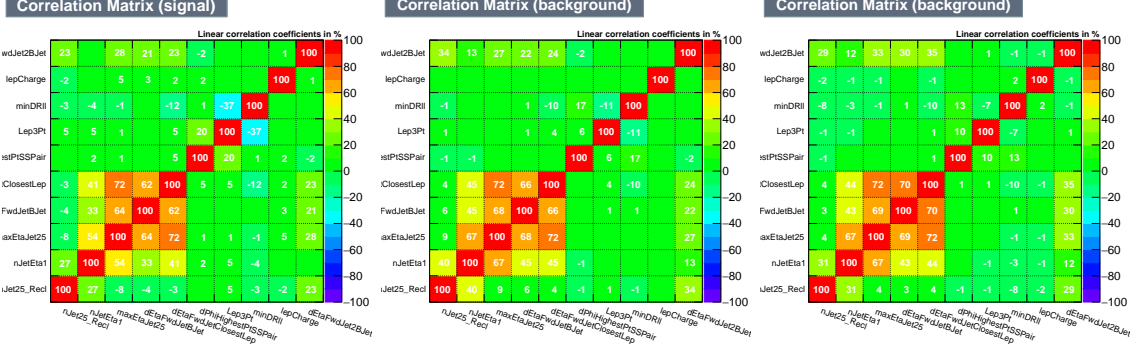


Figure 4.6: Signal (left), $t\bar{t}$ background (middle), and $t\bar{t}V$ background (right.) correlation matrices for the input variables in the TMVA analysis for the three lepton channel.

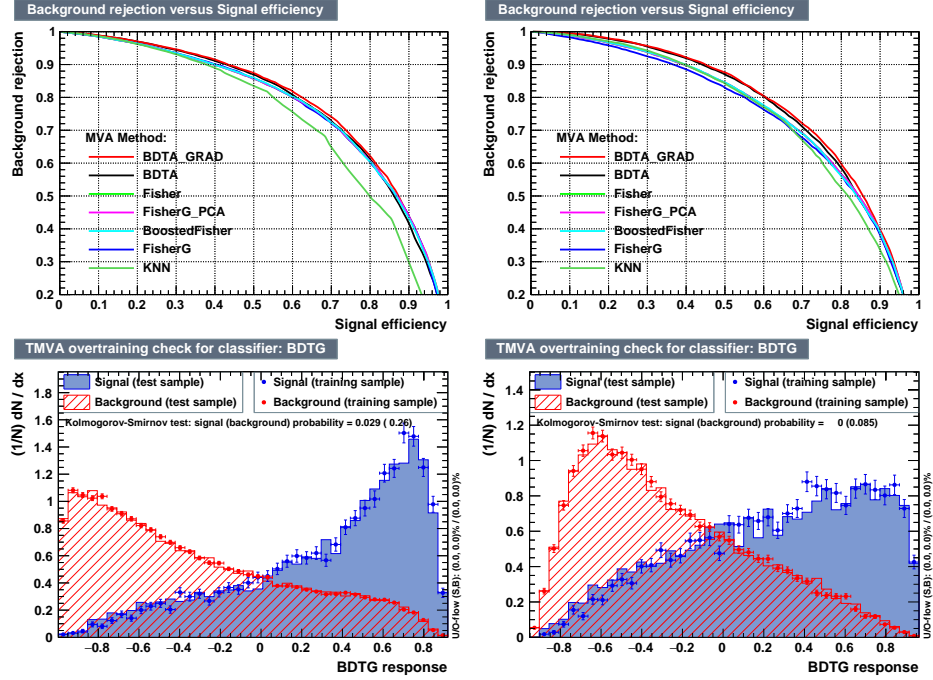


Figure 4.7: Top: background rejection vs signal efficiency (ROC curves) for various MVA classifiers (top) in the three lepton channel against $t\bar{t}V$ (left) and $t\bar{t}$ (right). Bottom: classifier output distributions for the gradient boosted decision trees, for training against $t\bar{t}V$ (left) and against $t\bar{t}$ (right).

1004 inator parameter values, with minimal overtraining. TMVA provides a ranking of the
 1005 input variables by their importance in the classification process, shown in Tab. 4.10.
 1006 The TMVA settings used in the BDT training are shown in Tab. 4.11.

ttbar training			ttV training		
Rank	Variable	Importance	Variable	Importance	Importance
1	minDRll	1.329e-01	dEtaFwdJetBJet	1.264e-01	
2	dEtaFwdJetClosestLep	1.294e-01	Lep3Pt	1.224e-01	
3	dEtaFwdJetBJet	1.209e-01	maxEtaJet25	1.221e-01	
4	dPhiHighestPtSSPair	1.192e-01	dEtaFwdJet2BJet	1.204e-01	
5	Lep3Pt	1.158e-01	dEtaFwdJetClosestLep	1.177e-01	
6	maxEtaJet25	1.121e-01	minDRll	1.143e-01	
7	dEtaFwdJet2BJet	9.363e-02	dPhiHighestPtSSPair	9.777e-02	
8	nJetEta1	6.730e-02	nJet25_Recl	9.034e-02	
9	nJet25_Recl	6.178e-02	nJetEta1	4.749e-02	
10	lepCharge	4.701e-02	lepCharge	4.116e-02	

Table 4.10: TMVA input variables ranking for BDTA_GRAD method for the trainings in the three lepton channel. For both trainings the rankings show almost the same 5 variables in the first places.

```

TMVA.Types.kBDT
NTrees=800
BoostType=Grad
Shrinkage=0.10
!UseBaggedGrad
nCuts=50
MaxDepth=3
NegWeightTreatment=PairNegWeightsGlobal
CreateMVApdfs

```

Table 4.11: TMVA configuration used in the BDT training.

1007 4.6 Additional discriminating variables

1008 Two additional discriminating variables were tested considering the fact that the
 1009 forward jet in the background could come from the pileup; since we have a real
 1010 forward jet in the signal, it could give some improvement in the discriminating power.
 1011 The additional variables describe the forward jet momentum (fwdJetPt25) and the
 1012 forward jet identification(fwdJetPUID). Distributions for these variables in the three
 1013 lepton channel are shown in the figure 4.8. The forward jet identification distribution
 1014 show that for both, signal and background, jets are mostly real jets.

1015 The testing was made including in the MVA input one variable at a time, so we

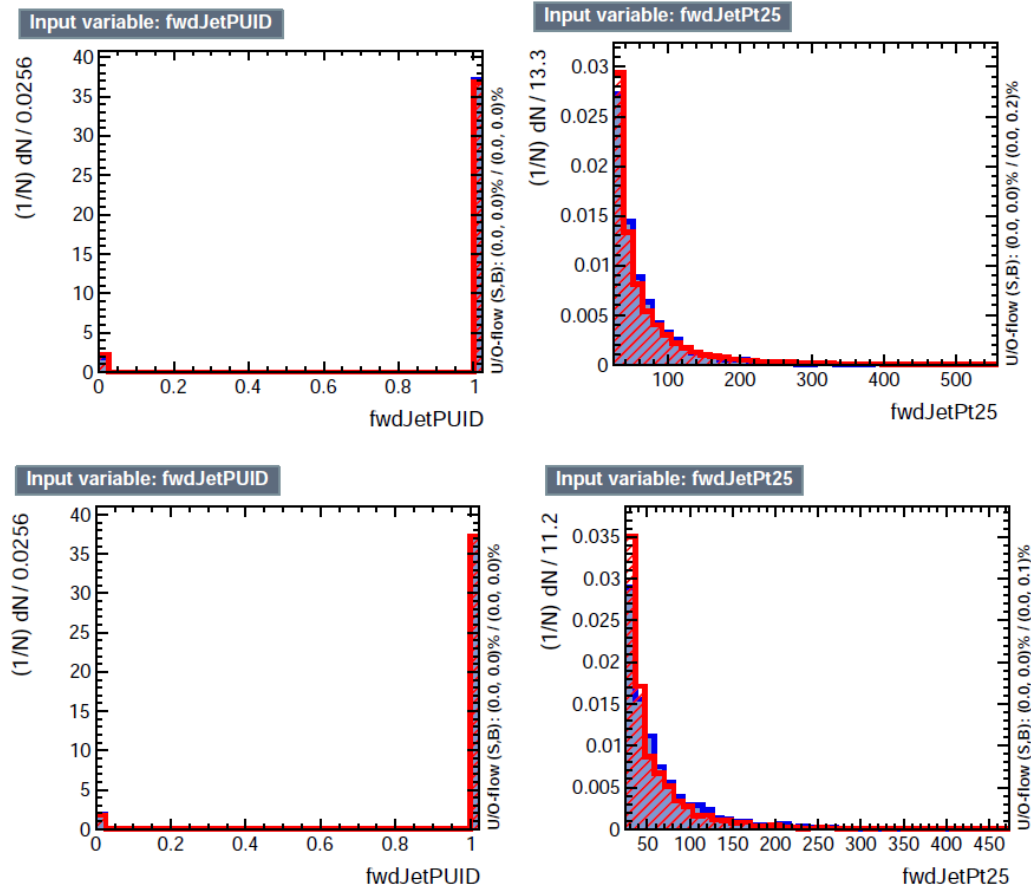


Figure 4.8: Additional discriminating variables distributions for ttV training (Top row) and tt training (bottom row) in the three lepton channel. The origin of the jets in the forward jet identification distribution is tagged as 0 for “pileup jets” while “real jets” are tagged as 1.

1016 can evaluate the discrimination power of each variable, and then both simultaneously.
 1017 fwdJetPUID was ranked in the last place in importance (11) in both training (ttV
 1018 and tt) while fwdJetPt25 was ranked 3 in the ttV training and 7 in the tt training.
 1019 When training using 12 variables, fwdJetPt25 was ranked 5 and 7 in the ttV and tt
 1020 trainings respectively, while fwdJetPUID was ranked 12 in both cases.

1021 The improvement in the discrimination performance provided by the additional
 1022 variables is about 1%, so it was decided not to include them in the procedure. Table
 1023 4.12 show the ROC-integral for all the testing cases we made.

ROC-integral	
base 10 var ttv	0.848
+ fwdJetPUID ttv	0.849
+ fwdJetPt25 ttv	0.856
12 var ttv	0.856
<hr/>	
base 10 var tt	0.777
+ fwdJetPUID tt	0.777
+ fwdJetPt25 tt	0.787
12 var	0.787

Table 4.12: ROC-integral for all the testing cases we made in the evaluation of the additional variables discriminating power. The improvement in the discrimination performance provided by the additional variables is about 1%

¹⁰²⁴ **Chapter 5**

¹⁰²⁵ **The CMS forward pixel detector**

¹⁰²⁶ **5.0.1 The phase 1 FPix upgrade**

¹⁰²⁷ **5.0.2 FPix module production line**

¹⁰²⁸ **5.0.3 The Gluing stage**

¹⁰²⁹ **5.0.4 The Encapsulation stage**

¹⁰³⁰ **5.0.5 The FPix module production yields**

1031 References

- 1032 [1] D.J. Griffiths, “Introduction to electrodynamics”. 4th ed. Pearson, (2013).
- 1033 [2] F. Mandl, G. Shaw. “Quantum field theory.” Chichester: Wiley (2009).
- 1034 [3] F. Halzen, and A.D. Martin, “Quarks and leptons: An introductory course in
1035 modern particle physics”. New York: Wiley, (1984) .
- 1036 [4] J.C. Maxwell. “A dynamical theory of the electromagnetic field”. Philosophical
1037 Transactions of the Royal Society of London. 155: 459â€¢512.(1865)
1038 doi:10.1098/rstl.1865.0008
- 1039 [5] M. Planck. “ÃIJber das Gesetz der Energieverteilung im Normalspektrum”.
1040 Annalen der Physik. 4 (3): 553.(1901).
- 1041 [6] A. Einstein “ÃIJber einen die Erzeugung und Verwandlung des Lichtes betref-
1042 fenden heuristischen Gesichtspunkt”. Annalen der Physik. 17 (6): 132â€¢148,
1043 (1905).
- 1044 [7] A. Einstein. “ÃIJber die von der molekularkinetischen Theorie der WÃdrme
1045 geforderte Bewegung von in ruhenden FlÃijssigkeiten suspendierten Teilchen”.
1046 Annalen der Physik. 17 (8): 549â€¢560, (1905).
- 1047 [8] A. Einstein. “Zur Elektrodynamik bewegter KÃürper”. Annalen der Physik. 17
1048 (10): 891â€¢921, (1905).

- 1049 [9] A. Einstein, "Ist die TrÄdgheit eines KÃürpers von seinem Energieinhalt ab-
 1050 hÃdngig?". Annalen der Physik. 18 (13): 639â€¢641, (1905).
- 1051 [10] B. P. Abbott et al. "Observation of Gravitational Waves from a Binary Black
 1052 Hole Merger". PRL 116, 061102 (2016).
- 1053 [11] J. Schwinger. "Quantum Electrodynamics. I. A Covariant Formulation". Phys-
 1054 ical Review. 74 (10): 1439â€¢61, (1948).
- 1055 [12] R. P. Feynman. "Spaceâ€¢Time Approach to Quantum Electrodynamics".
 1056 Physical Review. 76 (6): 769â€¢89, (1949).
- 1057 [13] S. Tomonaga. "On a Relativistically Invariant Formulation of the Quantum
 1058 Theory of Wave Fields". Progress of Theoretical Physics. 1 (2): 27â€¢42, (1946).
- 1059 [14] S.L. Glashow. "Partial symmetries of weak interactions", Nucl. Phys. 22 579-
 1060 588, (1961).
- 1061 [15] A. Salam, J.C. Ward. "Electromagnetic and weak interactions", Physics Letters
 1062 13 168-171, (1964).
- 1063 [16] S. Weinberg, "A model of leptons", Physical Review Letters, vol. 19, no. 21, p.
 1064 1264, (1967).
- 1065 [17] E. Noether, "Invariante Variationsprobleme", Nachrichten von der Gesellschaft
 1066 der Wissenschaften zu GÃüttingen, mathematisch-physikalische Klasse, vol.
 1067 1918, pp. 235â€¢257, (1918).
- 1068 [18] File:Standard_Model_of_Elementary_Particle_dark.svg. (2017, June 12)
 1069 Wikimedia Commons, the free media repository. Retrieved November 27,
 1070 2017 from <https://www.collegiate-advanced-electricity.com/single-post/2017/04/10/The-Standard-Model-of-Particle-Physics>.

- 1072 [19] M. Goldhaber, L. Grodzins, A.W. Sunyar “Helicity of Neutrinos”, Phys. Rev.
 1073 109, 1015 (1958).
- 1074 [20] Palanque-Delabrouille N et al. “Neutrino masses and cosmology with Lyman-
 1075 alpha forest power spectrum”, JCAP 11 011 (2015).
- 1076 [21] C. Patrignani et al. (Particle Data Group), Chin. Phys. C, 40, 100001 (2016)
 1077 and 2017 update.
- 1078 [22] M. Gell-Mann. “A Schematic Model of Baryons and Mesons”. Physics Letters.
 1079 8 (3): 214–215 (1964).
- 1080 [23] G. Zweig. “An SU(3) Model for Strong Interaction Symmetry and its Breaking”
 1081 (PDF). CERN Report No.8182/TH.401 (1964).
- 1082 [24] G. Zweig. “An SU(3) Model for Strong Interaction Symmetry and its Breaking:
 1083 II” (PDF). CERN Report No.8419/TH.412(1964).
- 1084 [25] M. Gell-Mann. “The Interpretation of the New Particles as Displaced Charged
 1085 Multiplets”. Il Nuovo Cimento 4: 848. (1956).
- 1086 [26] T. Nakano, K. Nishijima. “Charge Independence for V-particles”. Progress of
 1087 Theoretical Physics 10 (5): 581-582. (1953).
- 1088 [27] N. Cabibbo, “Unitary symmetry and leptonic decays” Physical Review Letters,
 1089 vol. 10, no. 12, p. 531, (1963).
- 1090 [28] M.Kobayashi, T.Maskawa, “CP-violation in the renormalizable theory of weak
 1091 interaction,” Progress of Theoretical Physics, vol. 49, no. 2, pp. 652-657, (1973).
- 1092 [29] File:Weak Decay (flipped).svg. (2017, June 12). Wikimedia Commons,
 1093 the free media repository. Retrieved November 27, 2017

- 1094 from [https://commons.wikimedia.org/w/index.php?title=File:Weak_Degay_\(flipped\).svg&oldid=247498592](https://commons.wikimedia.org/w/index.php?title=File:Weak_Degay_(flipped).svg&oldid=247498592).
- 1095 [30] Georgia Tech University. Coupling Constants for the Fundamental
1096 Forces(2005). Retrieved January 10, 2018, from <http://hyperphysics.phy-astr.gsu.edu/hbase/Forces/couple.html#c2>
- 1097 [31] M. Strassler. (May 31, 2013).The Strengths of the Known Forces. Retrieved
1098 January 10, 2018, from <https://profmattstrassler.com/articles-and-posts/particle-physics-basics/the-known-forces-of-nature/the-strength-of-the-known-forces/>
- 1099 [32] M. Peskin, D. Schroeder, “An introduction to quantum field theory”. Perseus
1100 Books Publishing L.L.C., (1995).
- 1101 [33] A. Pich. “The Standard Model of Electroweak Interactions”
1102 <https://arxiv.org/abs/1201.0537>
- 1103 [34] F.Bellaiche. (2012, 2 September). “What’s this Higgs boson anyway?”. Retrieved
1104 from: <https://www.quantum-bits.org/?p=233>
- 1105 [35] M. Endres et al. Nature 487, 454-458 (2012) doi:10.1038/nature11255
- 1106 [36] F. Englert, R. Brout. “Broken Symmetry and the Mass of Gauge Vec-
1107 tor Mesons”. Physical Review Letters. 13 (9): 321–323.(1964) Bib-
1108 code:1964PhRvL..13..321E. doi:10.1103/PhysRevLett.13.321
- 1109 [37] P.Higgs. “Broken Symmetries and the Masses of Gauge Bosons”. Physical
1110 Review Letters. 13 (16): 508–509,(1964). Bibcode:1964PhRvL..13..508H.
1111 doi:10.1103/PhysRevLett.13.508.

- 1116 [38] G.Guralnik, C.R. Hagen and T.W.B. Kibble. “Global Conservation Laws and
 1117 Massless Particles”. Physical Review Letters. 13 (20): 585–587, (1964). Bib-
 1118 code:1964PhRvL..13..585G. doi:10.1103/PhysRevLett.13.585.
- 1119 [39] CMS collaboration. “Observation of a new boson at a mass of 125
 1120 GeV with the CMS experiment at the LHC”. Physics Letters B.
 1121 716 (1): 30–61 (2012). arXiv:1207.7235. Bibcode:2012PhLB..716...30C.
 1122 doi:10.1016/j.physletb.2012.08.021
- 1123 [40] ATLAS collaboration. “Observation of a New Particle in the Search for
 1124 the Standard Model Higgs Boson with the ATLAS Detector at the LHC”.
 1125 Physics Letters B. 716 (1): 1–29(2012). arXiv:1207.7214. Bib-
 1126 code:2012PhLB..716....1A. doi:10.1016/j.physletb.2012.08.020.
- 1127 [41] ATLAS collaboration; CMS collaboration (26 March 2015). “Combined
 1128 Measurement of the Higgs Boson Mass in pp Collisions at $\sqrt{s}=7$ and
 1129 8 TeV with the ATLAS and CMS Experiments”. Physical Review Let-
 1130 ters. 114 (19): 191803. arXiv:1503.07589. Bibcode:2015PhRvL.114s1803A.
 1131 doi:10.1103/PhysRevLett.114.191803.
- 1132 [42] CMS Collaboration, “SM Higgs Branching Ratios and To-
 1133 tal Decay Widths (up-date in CERN Report4 2016)”.
 1134 <https://twiki.cern.ch/twiki/bin/view/LHCPhysics/CERNYellowReportPageBR>
 1135 , last accessed on 17.12.2017.
- 1136 [43] R.Grant V. “Determination of Higgs branching ratios in $H \rightarrow W^+W^- \rightarrow l^+l^- jj$ and $H \rightarrow ZZ \rightarrow l^+l^- jj$ channels”. Physics Department, Uni-
 1137 versity of Tennessee (Dated: October 31, 2012). Retrieved from
 1138 <http://aesop.phys.utk.edu/ph611/2012/projects/Riley.pdf>

- 1140 [44] LHC Higgs Cross Section Working Group, Denner, A., Heinemeyer, S. et al.
 1141 “Standard model Higgs-boson branching ratios with uncertainties”. Eur. Phys.
 1142 J. C (2011) 71: 1753. <https://doi.org/10.1140/epjc/s10052-011-1753-8>
- 1143 [45] CMS Collaboration, “Search for the associated production of a Higgs boson
 1144 with a single top quark in proton-proton collisions at $\sqrt{s} = 8$ TeV”, JHEP 06
 1145 (2016) 177, doi:10.1007/JHEP06(2016)177, arXiv:1509.08159.
- 1146 [46] B. Stieger, C. Jorda Lope et al., “Search for Associated Production of a Single
 1147 Top Quark and a Higgs Boson in Leptonic Channels”, CMS Analysis Note CMS
 1148 AN-14-140, 2014.
- 1149 [47] M. Peruzzi, C. Mueller, B. Stieger et al., “Search for ttH in multilepton final
 1150 states at $\sqrt{s} = 13$ TeV”, CMS Analysis Note CMS AN-16-211, 2016.
- 1151 [48] CMS Collaboration, “Search for H to bbar in association with a single top quark
 1152 as a test of Higgs boson couplings at $\sqrt{s} = 13$ TeV”, CMS Physics Analysis
 1153 Summary CMS-PAS-HIG-16-019, 2016.
- 1154 [49] B. Maier, “SingleTopHiggProduction13TeV”, February, 2016.
 1155 <https://twiki.cern.ch/twiki/bin/viewauth/CMS/SingleTopHiggsGeneration13TeV>.
- 1156 [50] M. Peruzzi, F. Romeo, B. Stieger et al., “Search for ttH in multilepton final
 1157 states at $\sqrt{s} = 13$ TeV”, CMS Analysis Note CMS AN-17-029, 2017.
- 1158 [51] B. WG, “BtagRecommendation80XReReco”, February, 2017.
 1159 <https://twiki.cern.ch/twiki/bin/view/CMS/BtagRecommendation80XReReco>.